

Cardiac glycosides are broad-spectrum senolytics

Ana Guerrero^{1,2}, Nicolás Herranz^{1,2}, Bin Sun^{1,2}, Verena Wagner^{1,2}, Suchira Gallage^{1,2,3}, Romain Guiho⁴, Katharina Wolter^{5,6}, Joaquim Pombo^{1,2}, Elaine E. Irvine^{1,2}, Andrew J. Innes^{1,2}, Jodie Birch^{1,2}, Justyna Glegola^{1,2}, Saba Manshaei⁴, Danijela Heide³, Gopuraja Dharmalingam^{1,2}, Jule Harbig^{5,6}, Antoni Olona⁷, Jacques Behmoaras⁷, Daniel Dauch^{5,6}, Anthony G. Uren^{1,2}, Lars Zender^{5,6,8}, Santiago Vernia^{1,2}, Juan Pedro Martínez-Barbera⁴, Mathias Heikenwalder³, Dominic J. Withers^{1,2} and Jesús Gil^{1,2*}

Senescence is a cellular stress response that results in the stable arrest of old, damaged or pre-neoplastic cells. Oncogene-induced senescence is tumour suppressive but can also exacerbate tumorigenesis through the secretion of proinflammatory factors from senescent cells. Drugs that selectively kill senescent cells, termed 'senolytics', have proved beneficial in animal models of many age-associated diseases. In the present study, we show that the cardiac glycoside ouabain is a senolytic agent with broad activity. Senescent cells are sensitized to ouabain-induced apoptosis, a process mediated in part by induction of the proapoptotic Bcl-2 family protein NOXA. We demonstrate that cardiac glycosides synergize with anti-cancer drugs to kill tumour cells and eliminate senescent cells that accumulate after irradiation or in old mice. Ouabain also eliminates senescent pre-neoplastic cells. The findings of the present study suggest that cardiac glycosides may be effective anti-cancer drugs by acting through multiple mechanisms. Given the broad range of senescent cells targeted by cardiac glycosides, their use against age-related diseases warrants further exploration.

Senescence is a protective stress response that limits the replication of damaged, pre-neoplastic or aged cells¹. Senescence can be induced by stresses including replicative exhaustion, oncogenic activation or exposure to genotoxic agents. On senescence induction, cells enter a stable cell cycle arrest, a process mediated by the upregulation of the cyclin-dependent kinase inhibitor p16^{INK4a} (ref. ²). Senescent cells also reorganize their chromatin, reprogram their metabolism, undergo changes in gene expression^{1,3}, and secrete a complex combination of factors collectively referred to as the senescence-associated secretory phenotype (SASP)⁴. The SASP has many roles^{5,6} and it is thought to mediate many of the pathophysiological consequences associated with senescence⁷.

Senescent cells are present in pre-neoplastic and fibrotic lesions, they accumulate in old tissues and are associated with an increasing list of pathologies⁸. Despite the fact that senescence protects against cancer and limits most types of fibrosis, the aberrant accumulation of senescent cells during ageing and disease is largely detrimental⁹. This negative role of senescent cells in ageing was first demonstrated with the help of genetic models that allow for the selective ablation of senescent cells^{10,11}. The use of these mouse models has shown that clearing senescent cells from progeroid or naturally ageing mice improves the healthspan¹⁰, increases the lifespan¹², and benefits an array of pathologies that include atherosclerosis¹³, osteoarthritis¹⁴ and neurodegenerative diseases^{15,16}.

These successful genetic studies prompted a search for drugs that can selectively kill senescent cells, termed 'senolytics'. Several senolytic compounds have been identified, including dasatinib and quercetin¹⁷, piperlongumine¹⁸, heat shock protein (HSP)-90

inhibitors¹⁹, or Bcl-2 family inhibitors such as ABT-263 (also known as navitoclax) and ABT-737 (refs. ^{20–22}). Currently, Bcl-2 family inhibitors are the most widely used senolytics, having been shown to be effective at killing a range of senescent cells in vivo and reproducing the effects observed in transgenic mice modelling senescence ablation²³. Bcl-2 inhibitors were initially developed as therapies for lymphoma. ABT-737 is a small molecule inhibitor of BCL-2, BCL-XL and BCL-W but has low solubility and oral bioavailability. ABT-263 inhibits the same molecules and is better suited for use in vivo, but it causes notable thrombocytopenia. Due to the important side effects associated with known senolytic compounds, there is a need to identify further compounds with senolytic properties. Despite the many roles that senescence plays in cancer initiation, progression and treatment, how senolytics can affect these processes is poorly defined. In the present study, we describe drug screens aimed at finding drugs that can target cells undergoing oncogene-induced and therapy-induced senescence. As a result, cardiac glycosides (CGs) were identified as a novel class of broad-spectrum senolytic compounds.

Results

A drug screen identifies ouabain as a broad-spectrum senolytic. In an effort to identify compounds modulating senescence, unbiased drug screens were carried out. First, IMR90 ER:RAS cells were used as a model of oncogene-induced senescence (OIS)²⁴. In these cells, activation of oncogenic RAS with 4-hydroxytamoxifen (4-OHT) induces senescence (see Extended Data Fig. 1a–c). We set up a screen to compare the effects that compounds have on the

¹MRC London Institute of Medical Sciences, London, UK. ²Institute of Clinical Sciences, Faculty of Medicine, Imperial College London, London, UK. ³Division of Chronic Inflammation and Cancer, German Cancer Research Centre, Heidelberg, Germany. ⁴Developmental Biology and Cancer Programme, Birth Defects Research Centre, Great Ormond Street Institute of Child Health, University College London, London, UK. ⁵Department of Internal Medicine VIII, University Hospital Tübingen, Tübingen, Germany. ⁶Department of Physiology I, Institute of Physiology, Eberhard Karls University Tübingen, Tübingen, Germany. ⁷Centre for Inflammatory Disease, Imperial College London, Hammersmith Hospital, London, UK. ⁸Translational Gastrointestinal Oncology Group, German Consortium for Translational Cancer Research, German Cancer Research Center, Heidelberg, Germany. *e-mail: jesus.gil@imperial.ac.uk

viability of control and senescent cells (Fig. 1a). It was confirmed that treatment with 1 μ M of the known senolytic ABT-263 preferentially eliminated cells undergoing OIS (Fig. 1b and see Extended Data Fig. 1d). By screening the LOPAC 1,280 library, comprising 1,280 pharmacologically active compounds, several drugs were identified that selectively killed cells undergoing Ras-induced senescence (Fig. 1c,d and see Extended Data Fig. 1e).

To understand whether the selective killing observed is specifically associated with activated RAS signalling or dependent on OIS, IMR90 E6/E7 ER:RAS cells were used. Papillomavirus E6 and E7 proteins interfere with the p53 and Rb pathways, respectively, and activation of RAS in these cells does not cause a senescence-associated growth arrest (see Extended Data Fig. 1f). Although most of the compounds tested (four of six: JFD00244, CGP-74514A, rotenone and rottlerin) did not selectively kill IMR90 E6/E7 ER:RAS cells, the other two (ouabain and diphenyleneiodonium) did (see Extended Data Fig. 1g).

Senescence can be triggered by a variety of insults that range from oncogenic activation to replicative stress or exposure to chemotherapeutic drugs^{1,2}. To identify senolytics targeting different types of senescence, a model of therapy-induced senescence (TIS, Fig. 1e) was screened. Treatment of IMR90 cells with etoposide caused senescence (see Extended Data Fig. 2a) and sensitized cells to death with 1 μ M ABT-263 (Fig. 1f). A screen using the LOPAC 1,280 library identified compounds that behaved as senolytics in TIS (Fig. 1g). By excluding toxic compounds and combining the data from both screens (Fig. 1h), it was observed that, although a subset of the identified drugs killed only cells undergoing either TIS or OIS (Extended Data Fig. 2b,c), others (indicated by the green box in Fig. 1h) selectively killed both types of senescent cells over their respective controls. On retesting, it was confirmed that CGP-74514A (a CDK1 inhibitor) and ouabain share this ability to selectively kill cells undergoing both OIS and TIS (Fig. 1i).

CGs induce apoptosis of senescent cells. Ouabain is a natural compound belonging to the CG family first described as a specific inhibitor of the Na⁺/K⁺ ATPase²⁵, although CGs are notoriously pleiotropic and can inhibit other targets²⁶. Ouabain treatment not only preferentially killed cells undergoing senescence triggered by oncogenic RAS (Fig. 1d) or etoposide (Fig. 1i), but also those exposed to doxorubicin (Fig. 2a) or the CDK4/6 inhibitor palbociclib (Fig. 2b), or undergoing replicative senescence (Fig. 2c). Mid-passage cultures of primary bronchial epithelial cells (PBECS) contain a mixture of senescent (p16^{INK4a}-positive) and normal (p16^{INK4a}-negative) cells. Treatment with ouabain or ABT-263 resulted in the selective elimination of p16^{INK4a}-positive cells (Fig. 2d). Taken together these results further demonstrate that ouabain behaves as a broad-spectrum senolytic agent.

For better understanding of the specificity of ouabain as a senolytic agent, we calculated its half-maximal effective concentration and observed that this was around 50-fold lower on senescent cells than on normal cells; we also confirmed that ouabain killed non-senescent cells with increased RAS signalling (see Extended Data Fig. 3a). Distinct CGs, such as digoxin and digitoxin, which are currently used for treating heart failure and atrial fibrillation²⁷, also behaved as senolytics (Fig. 2e,f). Importantly, digitoxin behaves as a senolytic at concentrations close to those observed in the plasma of cardiac patients treated with this drug (20–33 nM)²⁸ (Fig. 2f and see Extended Data Fig. 3b). These data suggest that senolytic effects may be achievable within the safe therapeutic dosing window for CGs.

Senescent cells have an increased lysosome mass and display higher activity of lysosomal enzymes including glycosidases such as β -galactosidase or α -fucosidase^{29,30}. To assess whether the glycoside chain of CGs could account for their differential effects on senescent cells, bufalin, a cardiac steroid that shares a similar structure to

CGs but lacks a glycoside chain, was tested. Bufalin also displayed senolytic properties (Fig. 2g), as did ouabagenin, the aglycone of ouabain (see Extended Data Fig. 3c,d). Furthermore, k-strophanthin and strophanthidin, another CG and its corresponding aglycone, shared a similar senolytic profile (see Extended Data Fig. 3e,f), arguing against an underlying role for the glycoside chain in the specificity of CGs towards senescent cells. CGs can trigger different types of cell death depending on the context. Treatment with CGs resulted in cleaved caspase-3 and induced caspase-3/7 activity in senescent cells (Fig. 2h and see Supplementary Fig. 1a). Moreover, the killing of senescent cells by CGs was prevented by pan-caspase inhibitors but not by inhibitors of ferroptosis, pyroptosis or necroptosis (Fig. 2i and see Supplementary Fig. 1b). The above results suggest that CGs behave as senolytic agents by preferentially triggering apoptosis in senescent cells.

Mechanism explaining the senolytic properties of CGs. CGs inhibit the Na⁺/K⁺ ATPase, a member of the P-type family of cation pumps that import two K⁺ in exchange for three Na⁺ molecules²⁵. Gene set enrichment analysis (GSEA) suggested that cells undergoing OIS are subjected to alterations in cellular chemical homeostasis (Fig. 3a). To better assess this, the intracellular concentrations of Na⁺ (Fig. 3b), Ca²⁺ (Fig. 3c) and K⁺ (Fig. 3d) were compared using fluorescent probes. Senescent cells displayed increased intracellular concentrations of all these cations. Interestingly, treatment with ouabain caused a more marked decrease of the intracellular levels of K⁺ in senescent than in normal cells, whereas supplementation with KCl prevented ouabain-induced (but not ABT-263-induced) death of senescent cells (Fig. 3e). Curcumin, a general inhibitor of P-type pumps³¹, also displayed senolytic activity (see Extended Data Fig. 4a), suggesting that the senolytic properties of CGs could be related to the inhibition of their canonical target, Na⁺/K⁺ ATPase, although it cannot be formally excluded that CGs induce senolysis via other cellular mechanisms. The rat Na⁺/K⁺ ATPase α_1 subunit (rATP1A1) harbours two point mutations at Gln¹¹¹ and Asn¹²² (analogous to those present in mouse Atp1a1) which reduce affinity to ouabain³². Overexpression of rATP1A1 prevented the senolytic effects of ouabain, but not those of ABT-263 (Fig. 3f).

To better understand the selectivity of CGs towards senescence, the transcriptome of senescent cells treated with CGs (see Extended Data Fig. 4b) was analysed. It was noted that both ouabain and digoxin induced a subset of proapoptotic Bcl-2 family proteins (Fig. 3g). An ouabain-dependent activation of JNK, GSK3- β and p38 was also observed in senescent cells (Fig. 3h). Knockdown experiments suggested that several Bcl-2 family proteins, most notably NOXA, mediated the senolytic actions of CGs (Fig. 3i and see Extended Data Figs. 4d and 4e,f). Treatment with inhibitors of JNK, GSK3- β or p38 signalling confirmed the involvement of these pathways on the induction of NOXA (Fig. 3j) and apoptosis in senescent cells treated with CGs (Fig. 3k). In summary, the above experiments suggest that senescent cells are more sensitive to apoptosis induced by CGs in a way that is partially dependent on NOXA.

Ouabain eliminates pre-neoplastic senescent cells. Murine cells are known to be more resistant to ouabain than human cells due to point mutations in the mouse Na⁺/K⁺ ATPase α_1 subunit (mAtp1a1)³². Although senescent mouse embryonic fibroblasts (MEFs) were not killed by high doses of ouabain, ouabain behaved as a senolytic in BNL CL.2 murine liver cells (see Supplementary Fig. 2), suggesting that mouse models can be used to assess the senolytic effects of ouabain in vivo. Cancer-associated senescent cells modulate tumour development and therapy response at multiple levels³³. Oncogene-induced senescence protects against tumour initiation^{34–37}. These pre-neoplastic senescent cells are the subject of active immune surveillance and failure of this process results in increased tumour risk⁵. To understand whether ouabain could potentiate the elimination of cells undergoing OIS, advantage was

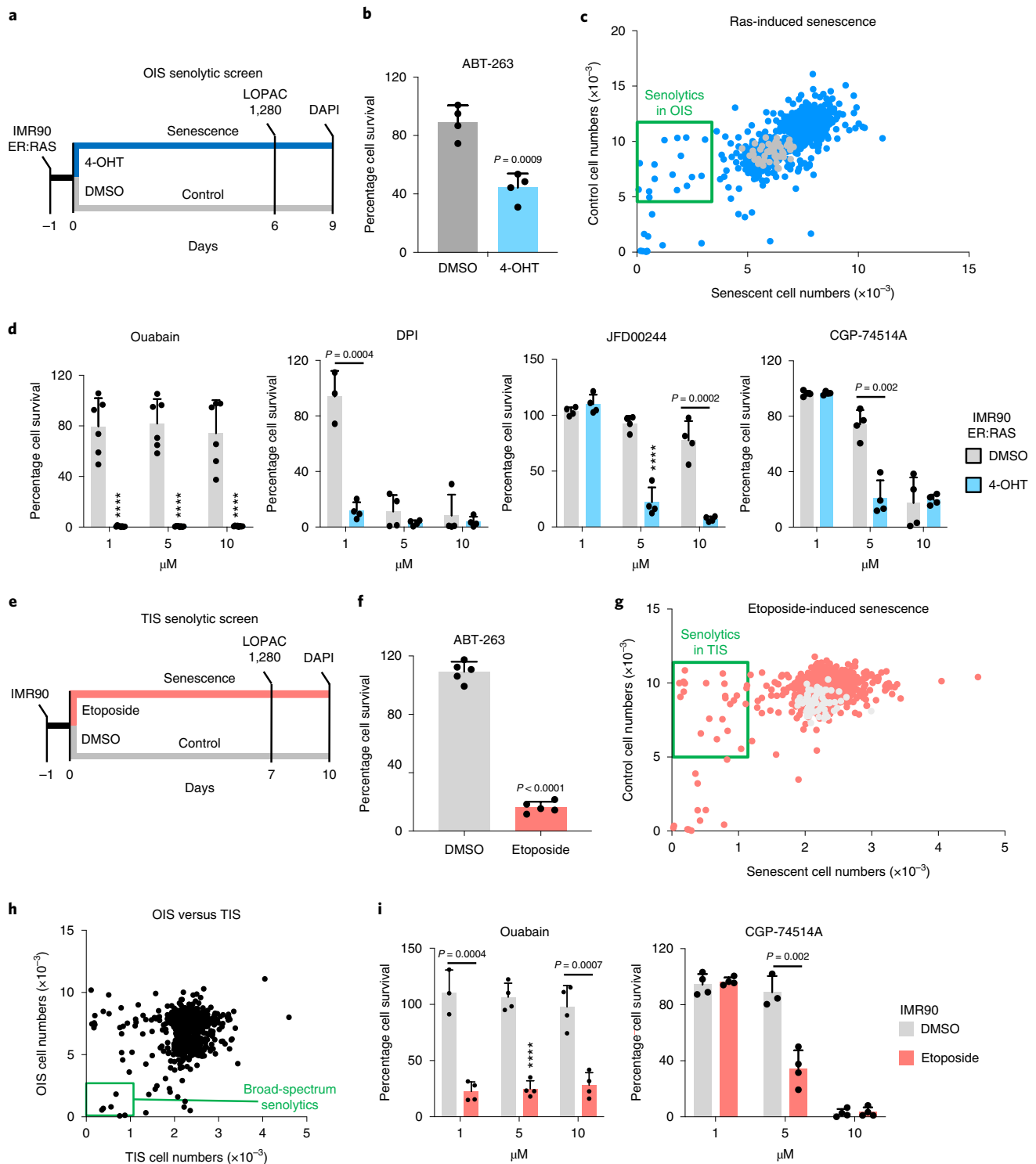


Fig. 1 | Drug screens identify ouabain as a broad-spectrum senolytic. **a**, Experimental design for the senolytic screen on oncogene-induced senescence. **b**, Quantification of cell survival of senescent and control IMR90 ER:RAS cells after treatment with 1 μM ABT-263 for 3 d ($n = 4$). **c**, Screen results. LOPAC 1,280 library compounds were assessed at 10 μM for 3 d. Hits were selected based on their ability to specifically kill senescent cells. Blue dots represent library drugs and grey dots represent DMSO controls. Each dot is the mean of three replicates. **d**, Senolytic activity of the indicated drugs in the context of oncogene-induced senescence in IMR90 ER:RAS cells ($n = 4$; $n = 6$ for ouabain; DMSO versus 4-OHT, **** $P < 0.0001$). **e**, Experimental design for the senolytic screen on therapy-induced senescence. **f**, Quantification of cell survival of senescent and control IMR90 cells after treatment with 1 μM ABT-263 for 3 d ($n = 5$). **g**, Screen results. LOPAC 1,280 library compounds were assessed at 10 μM for 3 d. Hits were selected based on their ability to specifically kill senescent cells. Red dots represent library drugs and grey dots represent DMSO controls. Each dot is the mean of three replicates. **h**, Comparison of senolytic activity for the LOPAC 1,280 library compounds in the context of OIS versus therapy-induced senescence. **i**, Senolytic activity of the indicated drugs in the context of therapy-induced senescence in IMR90 ($n = 4$; DMSO versus etoposide, **** $P < 0.0001$). All error bars represent mean \pm s.d.; n represents independent experiments. All statistical significances were calculated using unpaired, two-tailed, Student's *t*-tests and the Holm-Sidak method for multiple comparison tests.

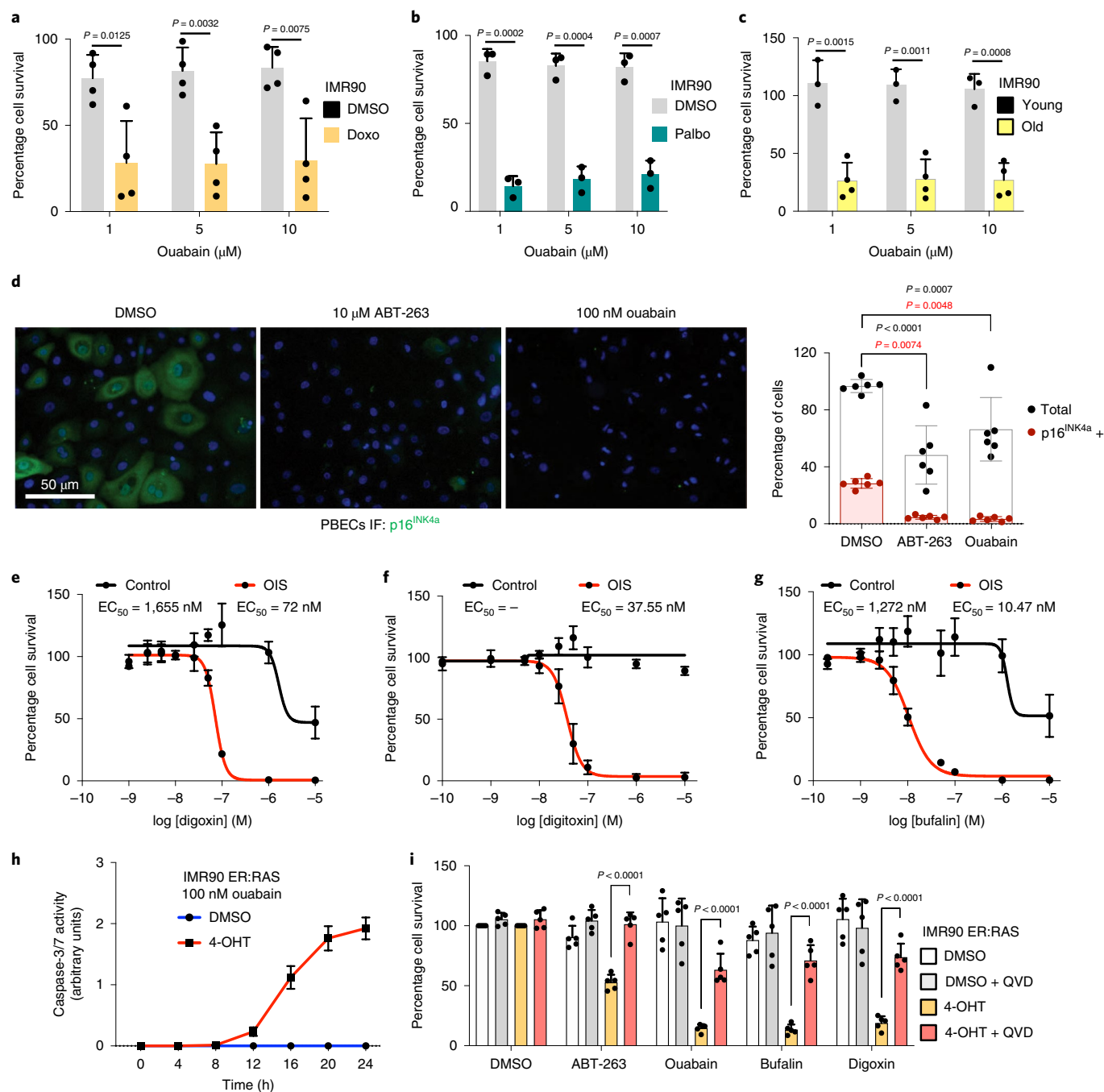


Fig. 2 | CGs induce apoptosis of senescent cells. **a–c**, Senolytic activity of ouabain in the context of therapy-induced senescence (doxorubicin, $n = 4$; palbociclib, $n = 3$) and replicative senescence ($n = 4$). Statistical significance was calculated using unpaired, two-tailed, Student's *t*-tests. **d**, Representative pictures (left) of IF staining for p16^{INK4a} in PBECs after treatment with ABT-263, ouabain or vehicle (DMSO); p16^{INK4a} is stained green. Scale bar, 50 μm . Quantification of total and p16^{INK4a}-positive PBECs (right, $n = 6$). Statistical significance was calculated using a two-way ANOVA (Dunnett's multiple comparisons test). Red stars refer to comparison of p16^{INK4a}-positive PBECs and black stars to comparison of total PBEC numbers. **e–g**, Dose-response analysis of senolytic activity of digoxin (**e**), digitoxin (**f**) and bufalin (**g**) in IMR90 ER:RAS cells ($n = 4$). EC_{50} , half-maximal effective concentration. **h**, Ouabain treatment of senescent cells induce caspase-3/7 activity. IMR90 ER:RAS cells were treated with 4-OHT or vehicle (DMSO) for 6 d to induce senescence. Then, 100 nM ouabain was added together with NuLight Rapid Red reagent for cell labelling and caspase-3/7 reagent for apoptosis (IncuCyte). Caspase-3/7 activity was measured at intervals of 4 h ($n = 3$). **i**, Pan-caspase inhibition (20 μM Q-VD-OPh) rescues senolytic activity of CGs (50 nM ouabain, 50 nM bufalin, 100 nM digoxin) and 1 μM ABT-263 on IMR90 ER:RAS cells ($n = 5$). Statistical significance was calculated using two-way ANOVA (Tukey's test). All error bars represent mean \pm s.d.; n represents independent experiments.

taken of a model of tumour initiation in the liver, in which senescence is induced in hepatocytes by transposon-mediated transfer of oncogenic *Nras* (*Nras*^{G12V})⁵. *Nras*^{G12V} was expressed in immunosuppressed mice (C.B-17 scid/beige) and a cohort was treated with

ouabain (Fig. 4a). Mice treated with CGs displayed reduced numbers of *Nras*-positive senescent hepatocytes due to increased apoptosis (Fig. 4b–e and see Extended Data Fig. 5), which validates the senolytic effects of CGs in vivo.

OIS is mostly considered as a tumour-suppressive mechanism but senescent cells present in the tumour microenvironment can also drive tumour progression. In this regard, it was recently shown that, in adamantinomatous craniopharyngioma, a clinically relevant pituitary paediatric tumour, clusters of β -catenin⁺ pre-neoplastic senescent cells positively influence tumour progression in a paracrine manner³⁸. A mouse model was used that drives the expression of oncogenic β -catenin in *Hesx1*⁺ embryonic precursors³⁹, and it was confirmed, as previously shown³⁸, that pre-neoplastic clusters of β -catenin-positive cells were senescent: they were arrested (ki67⁻) and enriched for markers of senescence such as p21^{Cip1} or Glb1 (the lysosomal β -galactosidase responsible for senescence-associated (SA)- β -galactosidase activity—see Supplementary Fig. 3). To understand whether ouabain could also eliminate these pro-tumorigenic senescent lesions, embryonic pituitaries at 18.5 d postcoitum (18.5 dpc) were dissected and cultured *ex vivo* with or without senolytics (Fig. 4f). Treatment with ABT-737 or ouabain specifically eliminated the β -catenin-positive senescent cells (Fig. 4g and see Extended Data Fig. 6a,b) without affecting other cell types in the pituitary, such as synaptophysin⁺ or adrenocorticotrophin hormone (ACTH)⁺ cells (see Extended Data Fig. 6a,c). Moreover, treatment with ouabain or digoxin reduced the levels of *Cdkn1a* (encoding for p21^{Cip1}), *Il1b* and *Il6* transcripts (see Extended Data Fig. 6d), suggesting that ouabain treatment resulted in reduced senescence and decreased SASP. Finally, co-staining with antibodies recognizing cleaved caspase-3 showed that ouabain selectively induced apoptosis of β -catenin⁺ senescent cells (Fig. 4h). The above results imply that CGs could be used as a prophylactic anti-cancer strategy to eliminate incipient pre-neoplastic cells.

Dual benefit of ouabain on therapy-induced senescence. Therapy-induced senescence plays an important role in determining the outcome of anti-cancer treatment⁴⁰, while also being responsible for some of its side effects⁴¹. Irradiation, chemotherapy and some targeted anti-cancer drugs, including aurora kinase inhibitors, all induce senescence^{40,42}. It has been proposed that a two-step combination of senescence-inducing anti-cancer agents followed by senolytics could be an improved strategy to treat cancer⁴³.

To investigate how CGs might behave in such a therapeutic protocol, SKHep1 liver cancer cells or A549 lung cancer cells were treated with senescence-inducing anti-cancer drugs. Treatment with etoposide (a topoisomerase II inhibitor), palbociclib (which inhibits CDK4/6), or the aurora kinase inhibitors barasertib, alisertib and tozasertib triggered senescence in SKHep1 and A549

cells (see Supplementary Figs. 4 and 5). Following the initial drug treatment, sequential use of ouabain, digoxin or ABT-263, a known senolytic²¹ (see Supplementary Fig. 4a), resulted in the efficient killing of senescent cancer cells (Fig. 5a–c and see Supplementary Fig. 5b). Similar results were obtained when two other liver cancer cells, Hun7 and HLF, were treated with alisertib followed by CGs (see Extended Data Fig. 7a,b). The sequential use of senescence-inducing drugs and CGs also killed melanoma (SK-Mel-5; see Extended Data Fig. 7c), breast cancer (MCF7; see Extended Data Fig. 7d) and colon cancer (HCT116; Fig. 5d) cells. Moreover, the use of syngeneic lines displaying reduced p53 expression (see Extended Data Fig. 7e,f) suggested that the effects were p53 independent (Fig. 5d and see Extended Data Fig. 7d). Finally, to assess whether the synergistic effects observed in the sequential treatments depended on senescence induction, advantage was taken of the multikinase inhibitor sorafenib. Treatment with sorafenib induced growth arrest, but not senescence, in SKHep1 and A549 cells (see Supplementary Figs. 4c and 5a,c,d), consistent with previous observations⁴⁴. Interestingly, it was noted that sequential treatment with ouabain did not result in enhanced killing of these cancer cells (see Supplementary Figs. 4c and 5e,f).

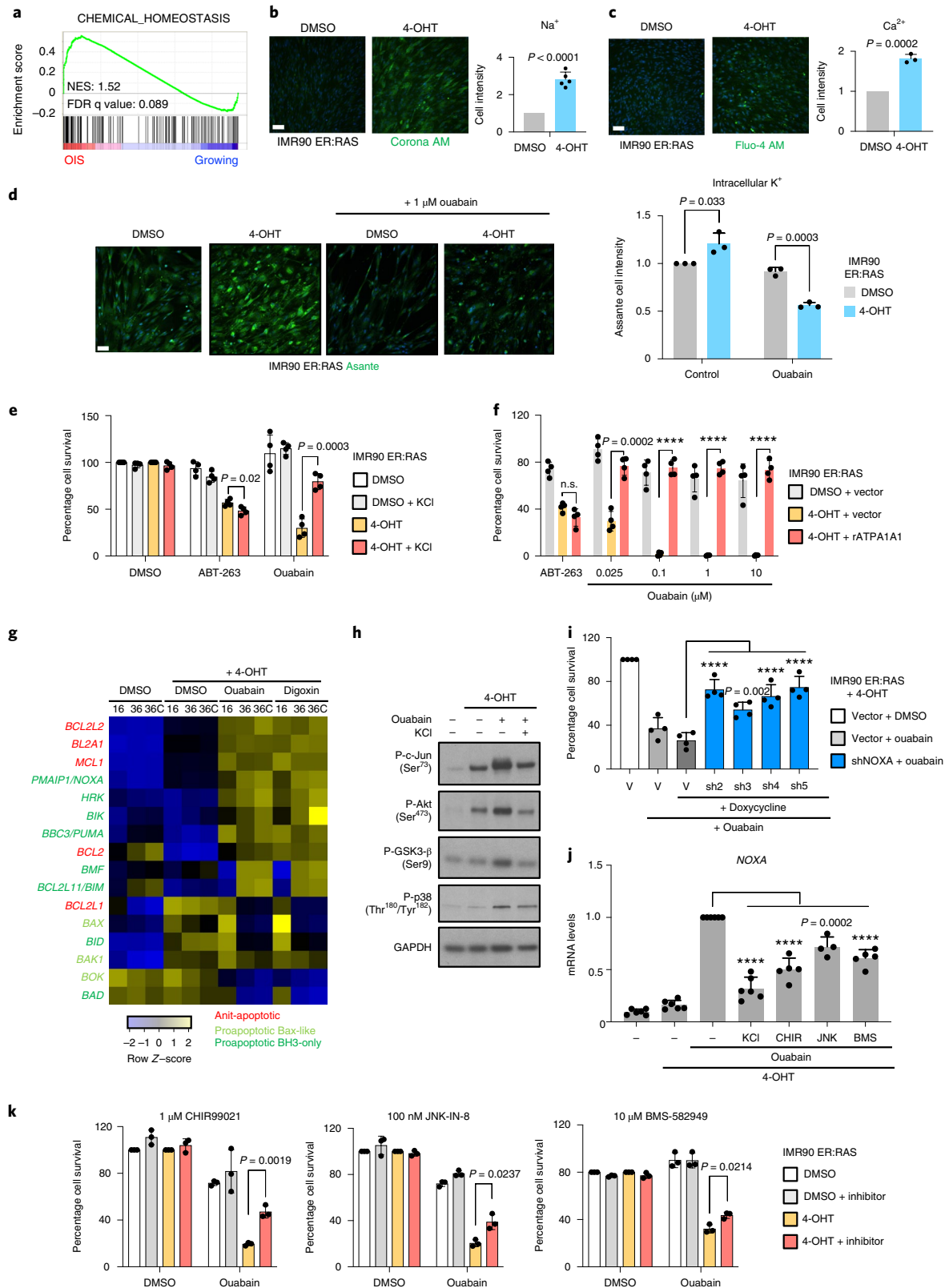
Although senescence plays an important role in the outcome of anti-cancer therapies, off-target induction of senescence by irradiation or chemotherapy can also partially explain their side effects⁴¹. To understand whether ouabain could also eliminate bystander senescent cells, mice were irradiated with 6 Gy (Fig. 5e). The lung was analysed, because it is the organ where the accumulation of senescent cells after irradiation is noted first⁴⁵. Treatment with ouabain resulted in a reduced presence of senescent cells and a lower expression of cytokines such as interleukin 1 α (IL-1 α) or IL-6 (Fig. 5f–h). A similar effect of ouabain on eliminating bystander senescent cells was observed in mice treated with doxorubicin (data not shown). The above results suggest that CGs can be combined with anti-cancer therapies to both enhance the elimination of cancer cells and avoid the accumulation of bystander senescent cells responsible for some of the side effects of these treatments.

Ouabain treatment resets immune infiltration in old mice. The accumulation of senescent cells in ageing organisms contributes to many diseases, including cancer⁴⁶. As CGs are broad-spectrum senolytics, the effect that they have on the elimination of senescent cells in old mice was investigated. To this end, 24-month-old female mice were subjected to a regimen of intermittent ouabain treatment (Fig. 6a). This regimen was well tolerated in mice, with

Fig. 3 | Mechanism explaining the senolytic properties of CGs. **a**, Chemical homeostasis GSEA signature in cells undergoing OIS compared with growing cells. **b,c**, Intracellular levels of Na⁺ ($n=5$) (**b**) and Ca²⁺ ($n=3$) (**c**) in IMR90 ER:RAS senescent cells compared with the corresponding controls. Representative pictures (left) and quantification (right) are shown. **d**, Intracellular levels of K⁺ in IMR90 ER:RAS senescent cells compared with the corresponding controls treated with 1 μ M ouabain for 18 h or with vehicle (DMSO) ($n=3$). Representative pictures (left) and quantification (right) are shown. **e**, Senolytic activity of 1 μ M ABT-263 and 50 nM ouabain assessed after supplementing the medium with 10 mM KCl ($n=4$). **f**, Senolytic activity of ABT-263 and ouabain assessed in IMR90 ER:RAS cells overexpressing the ouabain-insensitive rat ATP1A1 or an empty vector ($n=4$; 4-OHT + vector versus 4-OHT + rATP1a1; **** $P < 0.0001$). Statistical significance was calculated using the unpaired, two-tailed, Student's *t*-test (**b–f**). **g**, Heatmap showing the differential expression of *BCL-2* family genes in senescent compared with non-senescent cells after treatment with ouabain, digoxin or vehicle (DMSO). The timeline of the experiment is shown in Supplementary Fig. 5b. The 36C cells analysed 36 h post-CG treatment in the presence of caspase inhibitor (Q-VD-Oph). **h**, IMR90 ER:RAS cells were treated with 4-OHT or vehicle (DMSO) for 6 d to induce senescence. Cells were then treated with 1 μ M ouabain for 6 h, in the presence of 50 mM KCl or vehicle. Protein extracts were prepared. Immunoblots are a representative experiment out of three. **i**, IMR90 ER:RAS cells were infected with four different doxycycline-inducible shRNAs targeting NOXA ($n=4$; vector versus each different shRNA; **** $P < 0.0001$). Cells were subsequently treated with 4-OHT or vehicle (DMSO) for 6 d to induce senescence, and with 1 μ g μ l⁻¹ of doxycycline or vehicle (DMSO) to induce NOXA knockdown. Cells were then treated with 50 nM ouabain for 48 h. **j**, IMR90 ER:RAS cells were treated with 4-OHT or vehicle (DMSO) for 6 d to induce senescence. Cells were then treated with 50 nM ouabain for 20 h, in the presence of 50 mM KCl, GSK3- β inhibitor, JNK inhibitor, p38MAPK inhibitor or vehicle (DMSO). The effect of ouabain and all the different inhibitors on NOXA expression was determined using RT-qPCR ($n=5$; ouabain versus ouabain + inhibitors; **** $P < 0.0001$). Statistical significance was calculated using one-way ANOVA (Dunnett's test) (**i, j**). **k**, IMR90 ER:RAS cells were treated with 4-OHT or vehicle (DMSO) for 6 d to induce senescence. Cells were then treated with 50 nM ouabain for 48 h, in the presence of GSK3- β inhibitor, JNK inhibitor, p38MAPK inhibitor or vehicle (DMSO) ($n=3$). Quantification of cell survival was performed as described in Methods. The statistical significance was calculated using two-way ANOVA (Tukey's test). All error bars represent mean \pm s.d.; *n* represents independent experiments.

levels of ouabain in plasma reaching $1.24 \pm 0.48 \text{ ng ml}^{-1}$ 24 h after a round of treatment (see Extended Data Fig. 8a). Consistent with its known pharmacological properties⁴⁷, ouabain in blood dropped to undetectable levels at the end of the ‘holiday’ period. After five rounds of treatment, different metabolic parameters were measured in blood in a cohort of young mice and in old mice treated

with ouabain or saline as a control. Several age-associated changes were observed and there was a general trend to the reversal of such changes in mice treated with ouabain (Fig. 6b and see Extended Data Fig. 8b). For example, blood albumin levels, which are a general biomarker of well-being and fall during ageing and in a wide range of disease states⁴⁸, were decreased in old mice, a change that



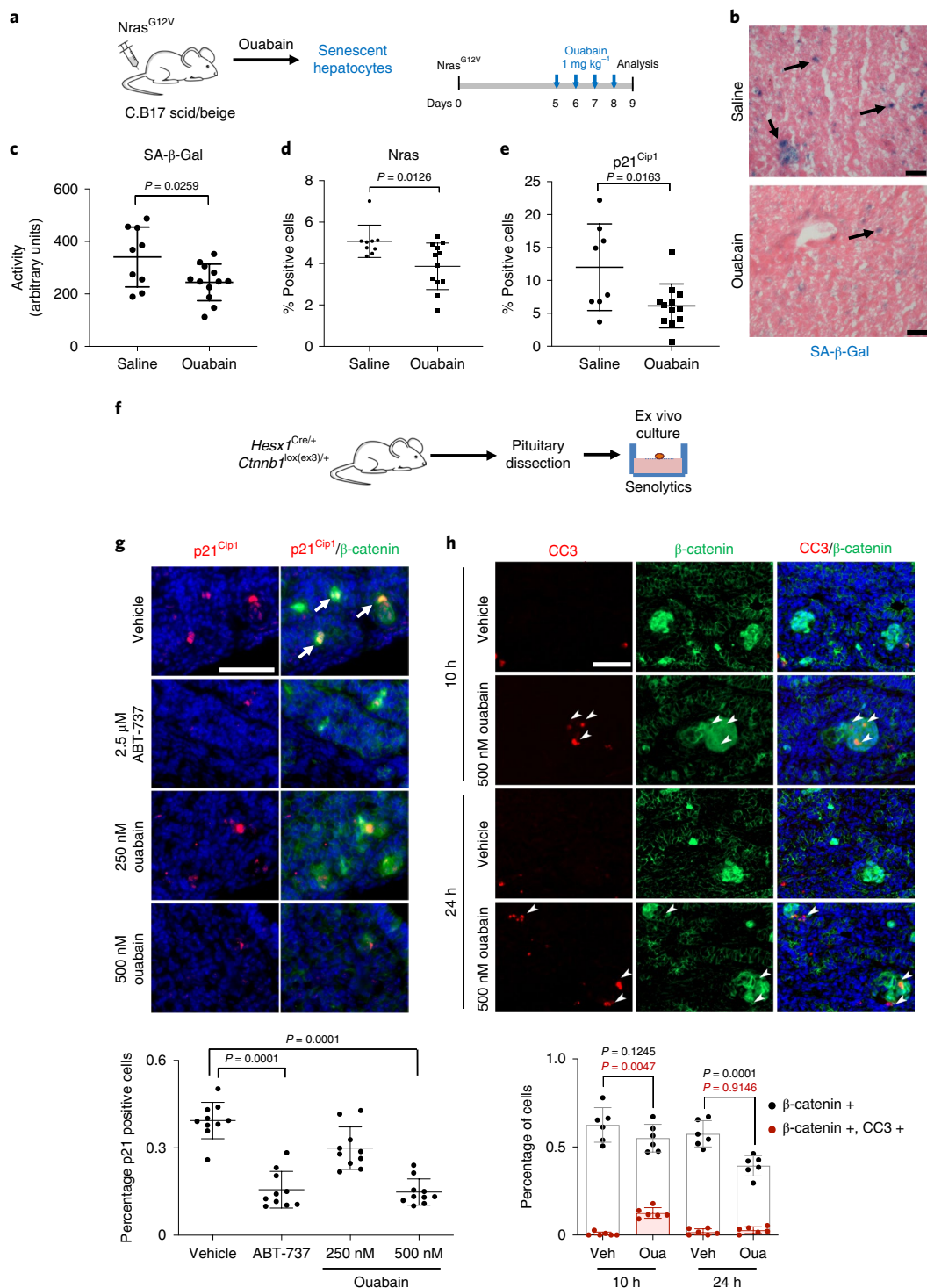


Fig. 4 | Ouabain selectively eliminates cells undergoing oncogene-induced senescence. **a**, Experimental design for the oncogene-induced senescence experiment in the liver. **b**, Representative images of SA-β-galactosidase (SA-β-Gal) staining in the liver. Arrows indicate examples of SA-β-galactosidase-positive cells. Scale bar, 50 μm. **c–e**, Quantification of SA-β-galactosidase activity (**c**), Nras-positive cells (**d**) and p21^{Cip1}-positive cells (**e**) in mice treated with vehicle ($n = 9$) or ouabain ($n = 12$). The statistical significance was calculated using the unpaired, two-tailed, Student's *t*-test. **f**, Experimental design for the senolytic experiment in an adamantinomatous craniopharyngioma mouse model. **g**, Tumoral pituitaries from 18.5 dpc *Hesx1*^{Cre/+};*Ctnnb1*^{lox(ex3)/+} mice were cultured in the presence of ABT-737 (2.5 μM), ouabain (250 nM and 500 nM) or vehicle (DMSO) and processed for analysis after 72 h ($n = 10$ mice per group). IF staining against β-catenin (green) and p21^{Cip1} (red). Arrows indicate examples of double-positive cells. Scale bar, 50 μm. Quantitative analysis of the IF demonstrates that ABT-737 and ouabain significantly reduce the number of β-catenin-positive and p21-positive cells. The statistical significance was calculated using Kruskal-Wallis and Dunn's multiple comparisons test. **h**, IF staining against β-catenin (green) and cleaved caspase-3 (CC3) (red) and quantitative analysis ($n = 6$ mice per group). Arrows indicate examples of double-positive cells. Scale bar, 50 μm. Veh, vehicle; Oua, ouabain. The statistical significance was calculated using two-way ANOVA (Tukey's multiple comparisons test). Red refers to comparison of double-positive cells and black to comparison of β-catenin-positive cells. Data represent mean ± s.d.; n represents number of mice; NS, not significant; ** $P < 0.01$; *** $P < 0.001$.

was notably reversed on treatment with ouabain (Fig. 6b). Similarly, blood phosphate levels were lower in old mice and this decrease was notably reversed on ouabain treatment (see Extended Data Fig. 8b). Trends in the ouabain-treated cohorts were also observed to reverse the increase in amylase observed in old mice (see Extended Data Fig. 8b). Furthermore, Rotarod activity, a marker of motor performance and coordination that declines with age, was improved on ouabain treatment (Fig. 6c). There was also a slight improvement in the grip strength in the treated group (see Extended Data Fig. 8c). To evaluate how ouabain treatment influences the presence of senescent cells in old mice, the expression of the senescent marker $p16^{Ink4a}$ was assessed in different tissues. Reduced $p16^{Ink4a}$ levels were observed when comparing ouabain-treated old mice with their age-matched counterparts in several tissues, including the liver, heart and kidney (Fig. 6d and see Extended Data Fig. 8d). In the liver, there was also a notable reduction in SA- β -galactosidase activity, suggesting that ouabain treatment diminished the number of senescent cells present in old mice (Fig. 6e). Consistent with this, we observed a decrease in other markers of senescence such as $p21^{Cip1}$ and also ORF1 protein expression of the LINE-1 transposon (see Extended Data Fig. 8g,h). Interestingly, whereas expression of the CG-resistant *Atp1a1* isoform is downregulated in the liver of old mice, the expression of a CG-sensitive isoform of the mouse Na^+/K^+ ATPase α_1 subunit, *Atp1a3*, increases (see Supplementary Fig. 6).

For further analysis of the impact of ouabain during ageing, RNA-sequencing (RNA-seq) experiments were carried out on these livers (Fig. 6f). Using GSEA analysis, the upregulation of gene signatures associated with senescence, inflammation and ageing in old mice was observed, a trend that notably reversed on ouabain treatment (Fig. 6f and see Extended Data Fig. 8e,f). Further, the transcriptome data were analysed using the xCell software, which predicts the cellular composition of the tissue⁴⁹. Using xCell, it was observed that the immune infiltration in the liver changed in old mice. Interestingly, many of these changes were notably reversed in ouabain-treated old mice (see Extended Data Fig. 9a). Some senolytic agents, such as Bcl-2 family inhibitors, affect the viability of specific immune cell populations, resulting in neutropenia and thrombocytopenia⁵⁰. To investigate whether changes in immune infiltration associated with ouabain treatment could be due to the selective killing of immune cell subsets, blood analysis was conducted at the end of the experiment. These studies did not reveal any significant alterations in the immune composition in blood on ouabain treatment (see Extended Data Fig. 9b), suggesting local effects on immune infiltration. This is in contrast with ABT-263 treatment which caused a drop of platelets in blood and decreased platelet infiltration in livers of mice (see Supplementary Fig. 7); this is consistent with what has been widely reported in human patients⁵⁰. To validate the predicted changes in immune infiltration on the livers of old mice treated with ouabain, immunohistochemistry staining of liver sections was carried out using different immune cell markers. Notable increases in the formation of myeloid (major histocompatibility complex II (MHC-II)⁺, CD68⁺ and F4/80⁺) and lymphoid (CD3⁺, CD4⁺, CD8⁺ and B220⁺) infiltrates were observed in livers of old compared with young mice.

This trend was reversed with ouabain treatment (Fig. 6g,h and see Extended Data Fig. 9c,d). In contrast, treatment with ouabain did not affect the increased infiltration of platelets (CD42b⁺) and granulocytes (Ly6G⁺) observed in old mice (see Extended Data Fig. 9c,d), therefore suggesting specificity. In conclusion, the above results suggest that ouabain can be used as a senolytic beyond cancer and that, besides eliminating senescent cells, ouabain reduced the levels of local inflammation and immune infiltration, which could have important effects on a wide range of pathologies.

Discussion

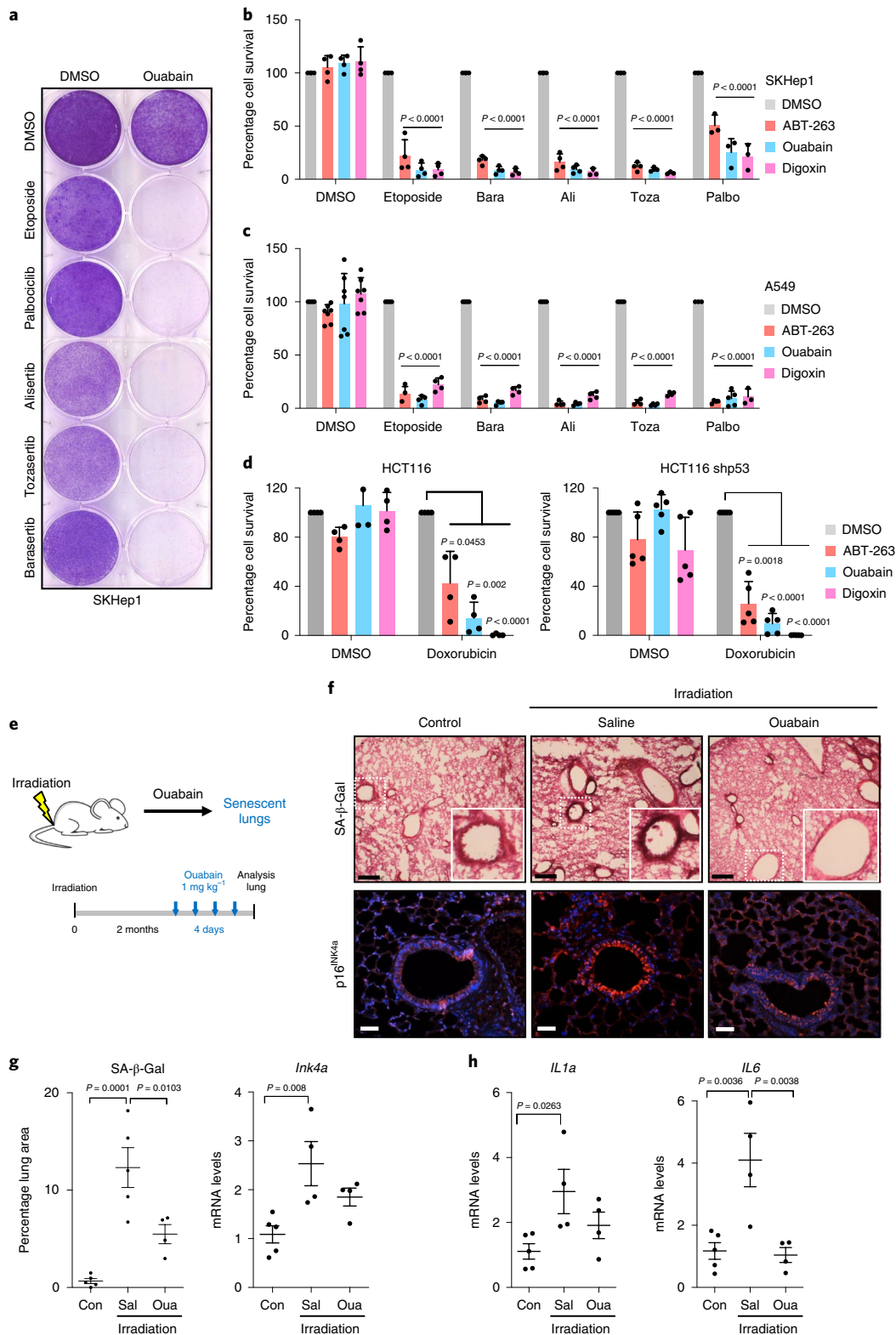
Senescent cells are associated with cancer, accumulate with age and are present in many pathologies⁹. Genetic and pharmacological strategies have demonstrated the benefits of eliminating senescent cells in the context of ageing and disease^{10,12,51}. Despite the multiple roles that senescence holds during cancer initiation, progression and treatment, how senolytics impact on these processes has not been studied enough. Senescence can be triggered by a variety of insults ranging from oncogenes to genotoxic stresses, inflammation or replicative exhaustion⁷. In the present study, screens were carried out for drugs preferentially killing cells undergoing oncogene-induced or therapy-induced senescence. A subset of the identified compounds behaves as broad-spectrum senolytics, whereas others are just selective against a specific type of senescent cells. These differences in specificity open up possibilities for the choice of senolytic, depending on its intended clinical use. One of the broad-specificity senolytics identified in the screen was ouabain, a natural compound belonging to the CG family. Ouabain also eliminates IMR90 E6/E7 ER:RAS cells that display increased RAS signalling, but do not undergo a senescence-associated growth arrest. This result suggests that ouabain is not just a senolytic compound, but also has a synthetic lethal interaction with RAS, which potentially makes it a cancer therapy with a useful dual mechanism of action. The results of the present study are consistent with those of the Collado group, which also identified CGs as senolytic in the context of bleomycin-induced senescence of cancer cells⁵². Similar to ouabain, other CGs such as digoxin and digitoxin, drugs currently used in clinical practice, selectively induce apoptosis of senescent cells. Importantly, digitoxin behaves as a senolytic at concentrations close to those observed in the plasma of cardiac patients treated with this drug (20–33 nM)²⁸, suggesting the potential use of CGs as senolytics in the clinic.

The broad-spectrum senolytic action of CGs suggest that they might target a common vulnerability induced by senescence. The canonical activity of CGs is to inhibit the Na^+/K^+ ATPase²⁵ but other activities have been suggested to explain their pleiotropic effects²⁶. Although the data of the present study suggest that the senolytic effects of CGs are due to on-target inhibition of the Na^+/K^+ ATPase, it needs to be clarified whether this inhibition (fully) explains the senolytic properties of CGs. Eventually, treatment with ouabain or digoxin results in elevated levels of several proapoptotic Bcl-2 family proteins. Among them, induction of NOXA explains in part how CGs trigger apoptosis in senescent cells.

Fig. 5 | Dual benefits of treatment with ouabain on therapy-induced senescence. **a**, Crystal violet-stained, six-well dishes of SKHep1 cells that underwent therapy-induced senescence (etoposide, palbociclib or aurora kinase inhibitors) and were subsequently treated with ouabain or vehicle (DMSO). The timeline of the experiment is shown in Supplementary Fig. 4a. Images are a representative experiment out of three. **b–d**, Quantification of cell survival of SKHep1 cells (**b**), A549 cells (**c**) or HCT116 cells (**d**) after treatment with the indicated drug combinations. The timeline of the experiment is shown in Supplementary Fig. 4a ($n = 4$). The statistical significance was calculated using two-way ANOVA (Tukey's test). **e**, Experimental design of the whole-body, irradiation-induced, senescence experiments. **f**, Representative IF images of $p16^{Ink4a}$ (bottom) and SA- β -galactosidase (SA- β -Gal) staining (top) in the lungs. Scale bar, 50 μ m. **g**, Quantification of area positive for SA- β -galactosidase staining and messenger RNA expression levels of $p16^{Ink4a}$ ($n = 5$ mock-irradiated control mice; $n = 4$ irradiated mice treated with ouabain; $n = 4$ irradiated mice treated with vehicle). **h**, Expression levels of *Il1 α* and *Il6* in lungs of non-irradiated mice ($n = 5$), irradiated mice treated with vehicle ($n = 4$) or irradiated mice treated with ouabain ($n = 4$). Con, control; Sal, saline; Oua, ouabain. The statistical significance was calculated using the unpaired, two-tailed, Student's *t*-test. Data represent mean \pm s.d.; *n* represents independent experiments in **b–d** and number of mice in **g, h**.

Mice have been described as more resistant than humans to the canonical effects of CGs due to differences in the *Atp1a1* protein³². Therefore, a conundrum arises as to why CGs behave as senolytics in mice. One possible explanation is that CGs act via a non-canonical activity. Alternatively, it was observed that the expression of the catalytic components of the Na^+/K^+ ATPase varies during ageing. Although CG-resistant *Atp1a1* is downregulated in the liver

of old mice, the expression of CG-sensitive *Atp1a3* increases (see Supplementary Fig. 6). Eventually, how CGs exert their senolytic effects and how much of the benefits observed on ouabain treatment of old mice are caused specifically by senolysis or via other effects will need to be clarified. In addition, whether the senolytic activity of CGs leads to improvements in other clinically relevant disease models associated with the accumulation of senescent cells,



including cancer models, or whether CGs have senolytic activity in humans, remains to be established. Senescence occurs at different stages of cancer evolution and treatment. OIS is a powerful tumour-suppressor mechanism^{34–37}. Therapy-induced senescence determines the response to chemo- and radiotherapy⁴⁰ while also contributing to their side effects⁴¹. The results of the present study suggest that treatment with CGs, and by extension with other senolytics, can have multi-stage beneficial effects in the context of cancer therapies.

Given that chemotherapy, radiotherapy and some targeted anti-cancer drugs rely on senescence induction, a follow-up senolytic treatment has been proposed as a way to improve cancer therapy⁴². The data of the present study suggest that broad-spectrum senolytics, such as CGs, will also eliminate other subsets of senescent cells, such as pre-neoplastic cells, bystander senescent cells induced by anti-cancer therapy and age-associated senescent cells that contribute to chronic inflammation. This broad eradication of senescent cells should result in additional benefits besides those derived from the direct effect on cancer cells. In particular, the fact that CGs will eliminate incipient pre-neoplastic cells should reduce the rate of cancer initiation and could suggest a prophylactic use to diminish cancer incidence. CGs have been used in the clinic for a long time. Digoxin and digitoxin are used for the treatment of heart failure and atrial arrhythmia. Interestingly, it has been suggested that CGs could be used as anti-cancer agents⁵³. In agreement with the results of the present study, a retrospective study showed that administration of digoxin during chemotherapy had a positive impact on overall survival in several cancer types⁵⁴. It was reasoned that the effect was due to the ability of CGs to induce immunogenic cell death. The results of the present study provide an additional explanation for those observations: CGs synergize with chemotherapy by killing senescent cells. Moreover, the broad specificity of CGs as senolytics, and the causal role of senescence in age-related disease, suggest that CGs might have benefits that extend beyond their anti-cancer properties. In this regard, studies in mice have shown that CGs reduced atherosclerosis⁵⁵ and ameliorated bleomycin-induced pulmonary fibrosis⁵⁶, which is consistent with senolytic activity. Given the pleiotropic effects of CGs, alternative or complementary explanations cannot be discarded beyond their senolytic effects, including direct killing of specific immune infiltrates.

We also showed that intermittent ouabain treatment reduced the number of senescent cells in old mice. In that context, ouabain not only targeted senescent cells, but also had a broader impact that was reflected in improved metabolic parameters and physical fitness. Moreover, the ouabain-induced reduction of senescence diminished chronic inflammation and reversed changes in immune infiltration observed in old mice. Importantly, those effects seem to be specific as ouabain treatment did not impact into granulocytes (Ly6G⁺) or platelets (CD42b⁺). These data constitute evidence of tissue remodelling happening in response to the elimination of senescent cells.

Despite the long-standing suggestions for novel clinical indications of CGs beyond heart disease, a factor limiting their use has been the potential for side effects. However, their senolytic action may require intermittent rather than continuous usage and, depending on the indication, administration could be local rather than systemic. The present study therefore suggests that the use of CGs as senolytics could be safer than initially thought. Given that digoxin has a long history of use in the clinic and its side effects can be monitored and managed⁵⁷, the pre-clinical data suggest that CGs should be trialled as senolytics in the context of cancer therapies and beyond.

Methods

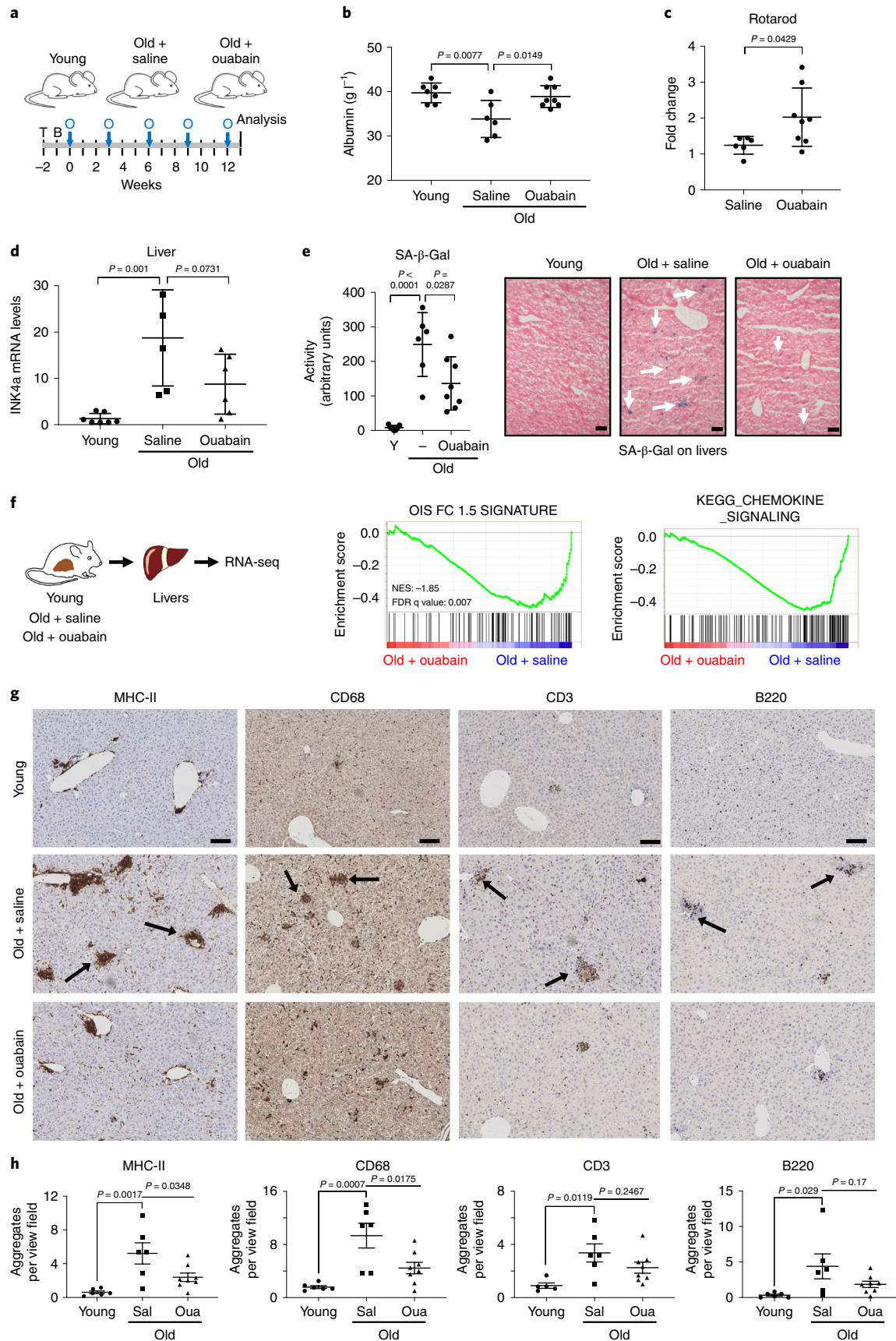
Drugs. The LOPAC 1,280 library was acquired from Sigma-Aldrich (LO1280). The following compounds were used in the present study: ABT-263 (Selleckchem, S1001), ouabain octahydrate (Sigma-Aldrich, O3125), diphenyleioidonium chloride (Sigma-Aldrich, D2926), JFD00244 (Sigma-Aldrich, J4829), CGP-745144 hydrochloride (Sigma-Aldrich, C3353), etoposide (Sigma-Aldrich, E1383), palbociclib HCl (Selleckchem, S1116), digoxin (Sigma-Aldrich, D6003), digitoxin (MedChemExpress HY-B1357), bufalin (Sigma-Aldrich, B0261), Q-VD-Oph hydrate (Sigma-Aldrich, SML0063), KCl (BioVision, 2115-100), doxycycline hydrate (Sigma-Aldrich, D9891), 4-OHT (Sigma-Aldrich, H7904), CHIR-99021 (Selleckchem, S2924), JNK-IN-8 (Selleckchem, S4901), BMS-582949 (Selleckchem, S8124), ABT-737 (Selleckchem, S1002), alisertib (Selleckchem, S1133), barasertib (Selleckchem, S1147), tozasertib (Selleckchem, S1048), doxorubicin hydrochloride (Cayman chemical, 15007), rotenone (Sigma-Aldrich, R8875), rottlerin (Sigma-Aldrich, R5648), calmidazolium chloride (Tocris, 2561), BIX-01294 (Selleckchem, S8006), mibefradil (Sigma-Aldrich, M5441), ouabagenin (Santa Cruz, sc-295983), strophanthidin (Sigma-Aldrich, S6626), strophanthin K (Sigma-Aldrich, S355445), lipoxstatin-1 (Selleckchem S7699), necrostatin-1 (Selleckchem S8037), belnacasan (VX-765; Selleckchem S2228), curcumin (Sigma-Aldrich, 08511) and sorafenib (Selleckchem S7397).

Antibodies. The following primary antibodies were used in this study: mouse monoclonal anti-bromodeoxyuridine (BrdU) (3D4; BD Biosciences, 55627) 1:2,000, rabbit polyclonal anti-glyceraldehyde 3-phosphate dehydrogenase (GAPDH) (Abcam, ab22555) 1:2,500, mouse monoclonal anti-p16^{INK4a} (JC-8; from CRUK) 1:1,000, rabbit polyclonal anti-p21 (M-19; Santa Cruz, sc-471) 1:200, rabbit monoclonal anti-phospho-c-Jun (Ser⁷³; D47G9, Cell Signaling Technology, 3270) 1:1,500, rabbit monoclonal anti-phospho-GSK3β (Ser⁹; D85E12, Cell Signaling Technology, 5558) 1:2,000, rabbit polyclonal anti-phospho-Akt (Ser⁴⁷³; Cell Signaling Technology, 9271) 1:2,000, rabbit polyclonal anti-phospho-p38 MAPK (Thr¹⁸⁰/Tyr¹⁸²; Cell Signaling Technology, 9211) 1:2,000, rabbit polyclonal anti-β-catenin (Thermo Scientific, RB-9035-P1) 1:500, mouse monoclonal anti-ACTH (Fitzgerald, N/A) 1:1,000, mouse polyclonal anti-p21 (BD Biosciences, 556431) 1:200, mouse monoclonal anti-synaptophysin (27G12; Leica, NCL-L-SYNAP-299) 1:250, rat anti-MHC-II (M5/114.15.2; Novus Biologicals, NBP1-43312) 1:500, rabbit polyclonal anti-CD68 (Abcam, ab125212) 1:100, rabbit monoclonal anti-CD3 (SP7; Zytomed, RBK024) 1:250, rat monoclonal anti-B220 (BD Biosciences, 553084) 1:3,000, rat monoclonal anti-F4/80 (Linaris, T2006) 1:120, rat monoclonal anti-CD4 (eBioscience, 14-9766) 1:1,000, mouse monoclonal anti-N-Ras (F155, Santa Cruz, sc-31), rabbit monoclonal anti-cleaved caspase-3 (Asp¹⁷⁵; 5A1E; Cell Signaling Technology, 9664) 1:400, rabbit monoclonal anti-LINE-1 ORF1p (EPR21844-108; Abcam, ab216324) 1:500, rat monoclonal anti-CD8α (Invitrogen, 14-0808-82) 1:200, rabbit monoclonal anti-CD42b (Abcam, ab183345) 1:200, rat Ly6g (BD Biosciences, 551459) 1:800, rabbit polyclonal anti-GLB1 (Proteintech, 15518-1AP) 1:100, rabbit monoclonal anti-Ki67 (Abcam, ab16667) 1:100 and rat monoclonal anti-green fluorescent protein (3H9, Chromotek) 1:200.

Fig. 6 | Ouabain resets immune infiltration in old mice. **a**, Experimental design for the ouabain treatment in old mice. T, time of enrolment; B, basal measures; O, ouabain treatment (3 consecutive days). **b**, Albumin levels of young ($n = 7$) and old mice, treated with either vehicle ($n = 6$) or ouabain ($n = 8$), were determined in whole-blood samples at the endpoint of the experiment. Data represent mean \pm s.d.; the unpaired, two-tailed, Student's t -test was used for statistical significance. **c**, Motor coordination, balance and strength of old mice treated with vehicle ($n = 6$) or ouabain ($n = 8$) assessed by performing the Rotarod test at 13 weeks after the start of the experiment. Represented is the fold change versus the basal test. Data represent mean \pm s.d.; the unpaired, two-tailed, Student's t -test was used for statistical significance. **d**, Expression levels of $p16^{\text{INK4a}}$ in liver was determined by RT-qPCR after treatment with vehicle ($n = 5$) or ouabain ($n = 6$). The mRNA expression levels in young mice ($n = 7$) were used as a reference. Data represent mean \pm s.d.; the unpaired, two-tailed, Student's t -test was used for statistical significance. **e**, Left, quantification of SA- β -galactosidase (SA- β -Gal) activity in the liver of young ($n = 7$) and old mice, treated with either vehicle ($n = 6$) or ouabain ($n = 8$). Right, representative images of SA- β -galactosidase activity in liver. Arrows indicate examples of SA- β -galactosidase-positive cells. Scale bar, 50 μm . Data represent mean \pm s.d.; the unpaired, two-tailed, Student's t -test was used for statistical significance. **f**, Left, experimental design for transcriptional profiling of livers from young or aged mice treated with ouabain or vehicle. Right, GSEA signature for oncogene-induced senescence and chemokines. **g,h**, Representative immunohistochemical images (**g**) and quantification (**h**) of the indicated immune cell markers in the liver of young ($n = 6$) and old mice, treated with either vehicle ($n = 6$) or ouabain ($n = 8$). Sal, saline; Oua, ouabain. Scale bar, 100 μm . Data represent mean \pm s.e.m.; the one-way ANOVA with Tukey's post-hoc comparison was used for statistical significance.

The following secondary antibodies were used: goat anti-mouse immunoglobulin (Ig)G (heavy plus light (H+L)), AlexaFluor 488 conjugated, Thermo Fisher Scientific, A11029), goat anti-mouse IgG (H+L), AlexaFluor

594 conjugated, Thermo Fisher Scientific, A11032), goat anti-rabbit IgG (H+L, AlexaFluor 594 conjugated, Thermo Fisher Scientific, A11037) and goat anti-rabbit IgG-horseradish peroxidase (Santa Cruz, sc-2004).



Cell lines. IMR90 (ATCC CCL-186), HEK-293T (ATCC CRL-11268), SK-HEP-1 (ATCC HTB-52), SK-MEL-5 (ATCC HTB-70), HCT116 (ATCC CCL-247), primary bronchial/tracheal epithelial cells (PBECs; ATCC PCS-300-010), MEF (ATCC SCRC-1008TM), MCF7 (ATCC HTB-22), BNL CL.2 (ATCC TIB-73) and A549 (ATCC CCL-185) cells were obtained from the American Type Culture Collection (ATCC). HLF (JCRB0405) and Huh7 (JCRB0403) cells were obtained from JCRB Cell Bank. IMR90 ER:RAS and IMR90 ER:RAS cells expressing E6 and E7 proteins of human papillomavirus (HPV)16 were generated by retroviral infection of IMR90 cells and have been described elsewhere^{38,39}. IMR90, SK-Hep-1, HCT116, MCF-7, BNL CL.2 cells and MEFs were cultured in Dulbecco's modified Eagle's medium (DMEM; Gibco) supplemented with 10% fetal bovine serum (FBS; Sigma) and 1% antibiotic-antimycotic solution (Gibco). A549 cells were cultured in DMEM supplemented with 10% FBS and 1% penicillin-streptomycin (Gibco). Sk-Mel-5 cells were cultured in RPMI medium 1640 (Gibco) supplemented with 10% FBS and 1% antibiotic-antimycotic solution. PBECs were cultured in airway epithelial cell basal medium (ATCC, PCS-300-030) supplemented with bronchial epithelial cell growth kit (ATCC, PCS-300-040). Huh7 and HLF cells were cultured in DMEM supplemented with 10% FBS, 1% penicillin-streptomycin, 1% non-essential amino acids (Gibco) and 1% sodium pyruvate (Gibco). To induce OIS, IMR90 ER:RAS cells were treated with 100 nM 4-OHT (Sigma) reconstituted in dimethylsulfoxide (DMSO). To induce chemotherapy-induced senescence IMR90 cells were treated with 0.5 μ M doxorubicin (Sigma) for 24 h, 50 μ M etoposide (Sigma) for 48 h or aurora kinase inhibitors (0.2 μ M tozasertib, 1 μ M alisertib, 1 μ M barasertib), for 7 d as described elsewhere⁴². To induce senescence by ionizing radiation, MEFs were γ -irradiated (10 Gy) and analysed at the indicated times.

Vector construction. The rat Na⁺/K⁺ ATPase α , subunit (rAlpha1) construct was a gift from Mauro Giacca (International Centre for Genetic Engineering and Biotechnology, Italy) and has been described before⁴⁰. To generate an rAlpha1 retroviral expressing vector, first the complementary DNA was PCR amplified using primers FwratATP1A1SnaB1 (5'-CGTACGTAGCCATGGGGAAGGGGTT-3') and RvratATP1A1Sall (5'-CGGTGACGCCCTAGTAGTAGGTTTCCT-3'), and the Platinum PCR SuperMix High Fidelity (Invitrogen) according to the manufacturer's instructions. Then, rAlpha1 cDNA was subcloned into a pBabe empty vector using standard techniques.

For de novo generation of miRE-based inducible short hairpin (sh)RNAs against NOXA, the human 97-mer oligonucleotides (IDT ultramers) coding for the respective shRNAs (shNOXA.2, PMAIP1_5366_1221; shNOXA.3, PMAIP1_5366_1235; shNOXA.4, PMAIP1_5366_574; shNOXA.5, PMAIP1_982) were PCR amplified using the primers miRE-Xho-fw (5'-TGAAGCTCGAAGGATATGCTGTGACAGTGAGCG-3') and miRE-EcoAIIg-rev (5'-TCTCGAATTCTAGCCCTTGAAGTCCGAGGCGAGTAGGC-3'), and the AccuPrime Pfx DNA Polymerase (Invitrogen) according to the manufacturer's instructions as described⁴¹. Amplification products were subsequently cloned into the pRRRL-TetON-Puro-Amp lentiviral backbone.

Retroviral and lentiviral infection. To generate IMR90 ER:RAS cells expressing rAlpha1 or inducible shRNAs against NOXA, human embryonic kidney HEK-293T cells were transfected with retroviral/lentiviral and packaging vectors using polyethylenimine (PEI) (PEI 2500, Polysciences). Two days after transfection, HEK-293T lentiviral supernatants were collected, filtered (0.45 μ M), diluted 1:4, supplemented with 4 μ g ml⁻¹ of polybrene and added to IMR90 ER:RAS cells plated the day before at a density of 1 million cells per 10-cm dish. After 4 h, lentivirus-containing media were replaced with fresh media. Two days after transfection, HEK-293T undiluted retroviral supernatants were collected, filtered (0.45 μ M) and supplemented with 4 μ g ml⁻¹ of polybrene and added to IMR90 ER:RAS cells plated the day before at a density of 1 million cells per 10-cm dish. After 3 and 6 h, fresh retrovirus-containing medium was added to the IMR90 ER:RAS cells. At 3 d after infection, all cells were passaged and cultured for 3 d in the presence of 1 μ g ml⁻¹ of puromycin (InvivoGen) to select for infected cells.

Growth assays. For BrdU incorporation assays, the cells were incubated with 10 μ M BrdU for 16–18 h and then fixed with 4% paraformaldehyde (PFA) (w/v). BrdU incorporation was assessed by immunofluorescence (IF) and high content analysis microscopy. For crystal violet staining, the cells were seeded at a low density on six-well dishes and fixed at the end of the treatment with 0.5% glutaraldehyde (w/v). The plates were then stained with 0.2% crystal violet (w/v).

IF staining of cells. Cells were grown in 96-well plates, fixed with 4% PFA (w/v), permeabilized in 0.2% Triton X-100 (v/v) diluted in phosphate-buffered saline (PBS) for 10 min, and blocked with 1% bovine serum albumin (BSA) (w/v) and 0.4% fish gelatin (v/v) (Sigma) for 30 min. Cells were then incubated with a primary antibody for 45 min, followed by the corresponding fluorescence-labelled secondary antibody (AlexaFluor) for 30 min and 1 μ g ml⁻¹ of DAPI for 15 min. Antibodies were diluted in blocking solution. After every step, cells were washed with PBS three times.

Cytochemical SA- β -galactosidase assay. Cells were grown on six-well plates, fixed with 0.5% glutaraldehyde (w/v) (Sigma) in PBS for 10–15 min, washed with 1 mM MgCl₂/PBS (pH 6.0) and then incubated with X-Gal staining solution (1 mg ml⁻¹

of X-Gal, Thermo Scientific, 5 mM K₃(Fe(CN)₆) and 5 mM K₄(Fe(CN)₆) for 8 h at 37 °C. Bright-field images of cells were taken using the DP20 digital camera attached to the Olympus CKX41 inverted light microscope. The percentage of SA- β -galactosidase-positive cells was estimated by counting at least 100 cells per replicate sample facilitated by the 'point picker' tool of ImageJ software (National Institutes of Health (NIH)).

For SA- β -galactosidase staining in tissues, frozen sections (6 μ m) were fixed in ice-cold 0.5% glutaraldehyde (w/v) solution for 15 min, washed with 1 mM MgCl₂/PBS (pH 6.0) for 5 min and then incubated with X-Gal staining solution for 16–18 h at 37 °C. After the staining, the slides were counterstained with eosin, dehydrated, mounted and analysed by phase-contrast microscopy. SA- β -galactosidase tissue staining was quantified using ImageJ software (NIH) by measuring the percentage of stained area in each section and multiplying it by its mean intensity value as described previously⁴². To exclude the luminal spaces in the lung sections, the percentage of the SA- β -galactosidase-positive area was divided by the total lung area, as determined by eosin-positive area using ImageJ.

Fluorescence SA- β -galactosidase assay. Cells were grown on 96-well plates and incubated with DDAOG (D-6488, Life Technologies) for 2 h. Cells were then fixed with 4% PFA for 15 min and nuclei were stained with 1 μ g ml⁻¹ of DAPI. Images were taken using a high-throughput fluorescent microscope IN Cell Analyzer 2000 (GE Healthcare) with a \times 20 objective. The percentage of SA- β -galactosidase-positive cells was estimated using the IN Cell Investigator v.2.7.3 software based on differences in cell intensity over an arbitrary threshold.

Determining senolytic activity. For oncogene-induced senescence experiments, IMR90 ER:RAS cells were plated in 96-well dishes and induced to undergo senescence by treating them with 100 nM 4-OHT for 6 d. At that point, 10 μ M of the indicated drugs was added, unless otherwise stated. In parallel, the same treatments were carried out in IMR90 ER:RAS cells treated with DMSO (–4-OHT). These cells do not undergo senescence. Cells were fixed at day 9 after 4-OHT induction and stained with 1 μ g ml⁻¹ of DAPI for 15 min to assess cell numbers using automated microscopy. Different models of senescence were used to test the senolytic compound activity in cell culture in a similar fashion. Briefly, for therapy-induced senescence IMR90 cells were treated with 50 μ M etoposide (48 h), 0.5 μ M doxorubicin (24 h) or left untreated, and then kept in drug-free complete medium until day 7, when the senolytics were added. Cells were fixed at day 10 after senescence induction. In all senescence types tested, a 3-d course of senolytics was applied. The percentage of cell survival was calculated by dividing the number of cells after drug treatment by the number of cells treated with vehicle.

For Huh7 and HLF, the cells were plated in six-well dishes and induced to undergo senescence by treating them with 500 nM alisertib for 4 d, removing the compound and allowing for establishment of senescence for another 4 d. For senolysis, compounds were subsequently added for 3 d at a concentration of 1 μ M or 5 μ M. Quantification of cell viability was done by collecting all the cells and determining the number of dead versus viable cells using trypan blue exclusion.

High content analysis. IF imaging was carried out using the automated high-throughput fluorescent microscope IN Cell Analyzer 2000 (GE Healthcare) with a \times 20 objective, with the exception of DNA damage foci analysis, which required a \times 40 objective. Fluorescent images were acquired for each of the fluorophores using built-in wavelength settings ('DAPI' for DAPI, 'FITC' for AlexaFluor 488 FITC, 'Texas Red' for AlexaFluor 594 and 'Cys' for DDAOG). Multiple fields within a well were acquired to include a minimum of 1,000 cells per sample well. High content analysis (HCA) of the images was processed using the IN Cell Investigator v.2.7.3 software as described previously⁴³. Briefly, DAPI served as a nuclear mask and hence allowed for segmentation of cells using a top-hat method. To detect cytoplasmic staining in cultured cells, a collar of 7–9 μ m around DAPI was applied. To detect cytoplasmic staining in tissue sections, a multiscale top-hat parameter was set on the reference wavelength (typically N-RAS staining). Nuclear IF in the reference wavelength, that is all the other wavelengths apart from DAPI, was quantified as an average of pixel intensity (grey scale) within the specified nuclear area. Cytoplasmic IF in the reference wavelength was quantified as a coefficient of variance of the pixel intensities within the collar area. Nuclear foci IF in the reference wavelength was quantified as the number of foci per nucleus. In samples of cultured cells, a threshold for positive cells was assigned above the average intensity of unstained or negative control samples, unless otherwise specified. In tissue sections, a threshold for positive cells was assigned above background staining using the built-in 'cell-to-background ratio' measurement. Immunohistochemistry imaging and quantification were also automated.

Gene expression analysis. Total RNA was extracted using TRIzol reagent (Invitrogen) and the RNeasy isolation kit (Qiagen). The cDNA was generated using random hexamers and SuperScript II reverse transcriptase (Invitrogen). Quantitative real-time PCR (RT-qPCR) was performed using SYBR Green PCR master mix (Applied Biosystems) in a CFX96 RT-PCR detection system (Bio-Rad). *GAPDH* or *RPS14* expression was used for normalization. Human primer pairs are: *PMAIP1*: ACCAAGCCGGATTGCGATT, ACTGCACTGTTCCTCGTGG *RPS14*: CTGCGAGTGCTGTAGAGG, TCACCGCCCTACATCAACT.

Mouse primer pairs are:

Gapdh: AACTTTGGCATTGTGGAAGG, ACACATTGGGGGTAGGAACA and ATGACATCAAGAAGGTGGTG, CATACCAGGAAATGAGCTTG
Il1a: CGCTTGAGTCGGCAAAGAAAT, TGGCAGAAGCTGAGTCTTCGT
Il6: TGATTGTATGAACAACGATGATGC, GGACTCTGGCTTTGTCTTTCTTG
Ink4A: CCCAACGCCCGAAGT, GCAGAAGAGCTGCTACGTGAA
Cxcl1: CTGGGATTCACCTCAAGAACATC, CAGGGTCAAGGCAAGCCTC
Rps14: GACCAAGACCCTGGACCT, CCCCTTTCTTCGAGTGCTA
Cdkn1a: CAGATCCACAGCGATATCCA, ACGGGACCGAAGAGACAAC
Il1β: TGCCACCTTTGACAGTGTATG, TGATGTCTGCTGCGAGATT
Il6: CAAGAAAGACAAGCCAGAGTC, GAAATTGGGGTAGGAAGGAC
Atp1a1: GGGGTTGGACGAGACAAGTAT, CGGCTCAAATCTGTTCCGTAT
Atp1a2: TGAGCTGGGCCGAAAATACC, GGTCCATCTCTAGCCAGAAT
Atp1a3: TCAGGGACCTCTTTCGACAAG, GCATCAGCTTTACGGAACCC.

Immunoblot. Cells were lysed in radioimmunoprecipitation assay buffer (80 mM Tris, pH 8.0, 150 mM NaCl, 1% Triton X-100, 0.5% sodium docusate, 0.1% sodium dodecylsulfate, 1 mM ethylenediaminetetraacetic acid) supplemented with one tablet of phosphatase and one tablet of protease inhibitors (Roche) per 10 ml radioimmunoprecipitation assay. Lysis was performed on ice for 20 min with occasional vortex, followed by centrifugation at 13,000g for 15 min at 4 °C to collect supernatant containing the protein extracts. Immunoblotting was carried out using a standard technique. Briefly, proteins were separated by size using precast gels (Bio-Rad) and then transferred to nitrocellulose membranes. The membranes were blocked for 1 h in PBS supplemented with 0.1% Tween 20 (v/v) and 5% BSA (w/v) (Sigma) and incubated with primary antibodies at 4 °C overnight. After three washes with PBS supplemented with 0.1% Tween 20 (v/v), the membranes were incubated with the corresponding secondary antibody conjugated with horseradish peroxidase and visualized using an ECL system (GE Healthcare) for chemiluminescent detection of the protein bands.

Transfection of siRNAs. IMR90 ER:RAS cells in suspension (100 μl) were reverse transfected with small interfering (si)RNAs (Dharmacon) on a well of a 96-well plate. The suspension medium was DMEM supplemented with 10% FBS only. The transfection mix for each sample contained 0.2 μl of DharmaFECT 1 (Dharmacon) in 17.4 μl of plain DMEM mixed with 3.6 μl of siRNA 30 min before cell seeding. Then, 18 h after transfection, the medium was replaced with fresh complete medium; 24 h after transfection, 50 nM ouabain or vehicle (DMSO) was added. The cells were fixed 72 h after transfection with 4% PFA (w/v) and stained with DAPI (1 μg ml⁻¹) for 15 min as previously described. The following siRNAs were acquired from Dharmacon and used in the present study: scrambled siRNAs (D-001210-01 and D-001210-02); siRNAs targeting the following human genes: *PMAIP1* (D-005275-07 and D-005275-08), *BBC3* (D-004380-05 and D-004380-06), *BMF* (D-004393-25 and D-004393-26), *HRK* (D-008216-04 and D-008216-05) and *BCL2L11* (D-004383-17 and D-004383-18).

IncuCyte analysis. IMR90 ER:RAS cells were plated in 96-well dishes and induced to undergo senescence as previously described. Different concentrations of ouabain and digoxin were added as usual. The cell culture medium was supplemented with IncuCyte NuLight Rapid Red reagent for cell labelling (Essen Bioscience) and IncuCyte caspase-3/7 reagent for apoptosis (Essen Bioscience). Four images per well were collected every 4 h for 3 d using a ×10 objective.

Measurement of intracellular ions. Intracellular K⁺, Na⁺ and Ca²⁺ were measured using Asante Potassium Green-2 AM (Abcam, 2 μM), CoroNa Green, AM (Invitrogen, 5 μM) and the Fluo-4 AM (Invitrogen, 2 μM) probes, respectively. Cells were incubated with the probes for 30 min (CoroNa Green and Fluo-4) or 60 min (Asante Potassium Green-2 AM). Probes were diluted in Hank's balanced salt solution (Sigma). After treatment, cells were washed and fixed with 4% PFA (w/v) as usual for Asante Potassium Green-2 AM and CoroNa Green. For cells incubated with Fluo-4 AM, they were incubated with Hoechst stain (1 μg ml⁻¹) for the last 10 min of the incubation and imaged alive.

Mouse models and drug treatments. All mice were purchased from Charles River UK, Ltd. For induction of senescence, C57BL/6J mice aged 8–12 weeks were exposed to a sublethal dose (6 Gy) of total body irradiation. Then 8 weeks later, the mice were injected with 1 mg kg⁻¹ of ouabain (intraperitoneally (i.p.)) or vehicle for 4 consecutive days. Mice were killed 24 h after the last injection. Mice lungs were harvested for RNA extraction, paraffin embedded for immunohistology or frozen in optimal cutting temperature (OCT)/Sucrose 15% (1:1) solution for cryosectioning and SA-β-galactosidase stains. The mice used for all experiments were randomly assigned to control or treatment groups. Both sexes were used throughout the study.

For in vivo treatment, ABT-263 was prepared in ethanol:polyethylene glycol 400 (PEG 400):Phosal 50 PG at 10:30:60, as previously described⁴⁵. Mice were gavaged with vehicle (ethanol:PEG 400:Phosal 50 PG) or ABT-263 (50 mg kg⁻¹). Peripheral whole-blood and liver samples were collected 6 h after dosing.

Female C57BL/6J mice aged 98–103 weeks at the start of the experiment (they were not littermates) were treated with 1 mg kg⁻¹ of ouabain (i.p.) (n = 9) or vehicle

(n = 7) for 13 weeks. Mice were injected three times a week every other day (days 1, 3 and 5). Every week of treatment was followed by 2 weeks of rest (except for the experimental endpoint). A group of young female C57BL/6J mice (10 weeks old) was used as reference. Mice were trained twice for all the physical tests before starting treatment. Tests were always performed the week after ouabain treatment.

Female C.B-17 SCID/beige (CB17.Cg-Prkdc^{scid}Lyst^{bg-1}/CrI) mice were injected at age 5–8 weeks. Vectors for hydrodynamic injection were prepared using the Sigma-Aldrich GenElute HP Endotoxin-Free Plasmid Maxiprep Kit. Transposon-mediated gene transfer was as previously described³; briefly 20 μg of the indicated vector containing Nras^{G12V} and 5 μg of SB13 transposase-expressing plasmid were diluted in sterile-filtered PBS to a total volume of 10% of the body weight of the animal, before being injected into the lateral tail vein in under 10 s. Then, 5 d after hydrodynamic tail vein injection (HTVI), mice were treated with 1 mg kg⁻¹ of ouabain (i.p.) or vehicle for 4 consecutive days. The mice were randomly assigned to a control or treatment group; 24 h after the last injection of the drug (9 d after HTVI) the mice were culled and the livers collected. All mouse procedures were performed under licence, following the UK Home Office Animals (Scientific Procedures) Act 1986 and local institutional guidelines (University College London or Imperial College ethical review committees).

Physical tests. The Rotarod apparatus (Ugo Basile) was used to measure fore- and hindlimb motor coordination, balance and strength. Mice received three trials a day with an intertrial interval of 1 h for 3 consecutive days. The rod accelerated from 5g to 60g over a period of 570 s and the latency to fall was recorded. For the subsequent analysis, the mean latency was taken for the nine trials and plotted as a value for the week.

A grip strength meter was used to measure forelimb strength. To measure grip strength, the mouse is swung gently by the tail so that its forelimbs contact the bar. The mouse instinctively grips the bar and is pulled horizontally backwards, exerting a tension. When the tension becomes too great, the mouse releases the bars. The maximum load is recorded by the grip strength meter, which is then returned to zero before the next test. The mouse is placed in its home cage for a minute to rest before the next test. Each mouse performs five consecutive tests, and the three best scores are used for statistical analysis. This protocol is preferred because lower scores are often due to the mouse failing to grip the bar effectively, rather than reflecting muscular strength.

Vetscan VS2 for analysis of blood parameters. Whole blood was collected into lithium-heparin-coated tubes (Abaxis) from the carotid artery after cervical dislocation of the mice; 120–140 μl of whole blood was then added into the comprehensive diagnostic profile rotor for geriatric testing (Abaxis) and run on the VetScan VS2 Chemistry Analyzer (Abaxis).

Peripheral whole-blood analysis of immune cell composition. Blood was collected using citrate or ethylenediaminetetraacetic acid (Microvette CB 300 K2E, Sarstedt) as an anticoagulant from tail-vein whole blood and diluted using saline to a volume of at least 200 μl. Complete blood counts were obtained using the Sysmex XE2100 automated cell counter.

Immunohistochemistry staining of liver sections. Livers were fixed overnight in 4% PFA before embedding and sectioning. Paraffin-embedded liver sections (2 μm) were processed for immunohistochemistry thereafter. Automated staining was performed on BOND-MAX (Leica Biosystems). Antigen retrieval was carried out using Bond citrate solution (AR9961, Leica), Bond ethylenediaminetetraacetic acid solution (AR9640, Leica) or Bond proteolytic enzyme kit (AR9551, Leica), after which sections were incubated with antibodies against antigens in Bond primary antibody diluent (AR9352, Leica Biosystems). Primary antibody exposure was followed by secondary antibody (Leica Biosystems) and staining using the Bond Polymer Refine Detection Kit (DS9800, Leica Biosystems). For quantification of stainings, slides were scanned using a SCN400 slide scanner (Leica Biosystems) at ×20 magnification.

ELISA for ouabain. C57BL/6J mice were treated with 1 mg kg⁻¹ of ouabain (i.p.) for 4 consecutive days. Then, 24 h after the last injection, blood was collected from the tail vein using lithium-heparin-coated Microvette tubes (Sarstedt CB300 LH). Samples were centrifuged at 2,000g for 5 min at room temperature and the supernatant was collected as plasma for subsequent ELISA analysis (Cloud-Clone Corp., CEV857Ge).

Ex vivo culture of mouse pituitaries. Neoplastic pituitaries were dissected from *Hexx1*^{Cred/+}; *Ctnnb1*^{lox(ex3)/+} embryos at 18.5 dpc. Wild-type pituitaries were dissected from *Hexx1*^{+/+}; *Ctnnb1*^{lox(ex3)/+} embryos at 18.5 dpc. The sex was not determined. These embryos were obtained in the same litters by crossing *Hexx1*^{Cred/+} males aged 2–6 months (MGI:3822473 (ref. 64); C57BL/6 background) with *Ctnnb1*^{lox(ex3)/lox(ex3)} females aged 2–6 months (MGI:1858008 (ref. 65); C57BL/6 background). The genotype was assessed by phenotypic discrimination. After dissection, pituitaries were placed on top of 0.2-μM Whatman filters (SLS) in 24-well plates containing 500 μl of medium (DMEM-F12 (Gibco), 1% penicillin-streptomycin (Sigma) and 1% FBS (PAA)) supplemented with ABT-737 (2.5 μM), ouabain (250 nM

and 500 nM) or vehicle (DMSO). The medium was changed every 24 h, and the pituitaries were processed for analysis after 72 h. IF staining was performed as previously described³⁶. The proportion of β -catenin-accumulating and p21-positive cells was calculated as an index of the total DAPI-stained nuclei. The proportion of β -catenin-accumulating, cleaved-caspase-3- and p21-positive cells was calculated as an index of the total DAPI-stained nuclei. Over 300,000 DAPI nuclei were counted from 10 histological sections per sample, in a total of 12 neoplastic pituitaries. For gene expression analysis, after 72 h of ex vivo culture, pituitaries were passed through a Qiashtredder column (Qiagen) and processed for total RNA extraction using the RNeasy Micro kit (Qiagen). Then, 150 ng of total RNA was reverse transcribed to cDNA using the Transcriptor First Strand cDNA Synthesis Kit and random hexamers (Roche).

RNA-seq analysis. The quality of the raw sequencing reads was assessed using FASTQC. Human RNA-sequencing (RNA-seq) samples were aligned to human genome hg19 by using Tophat (v.2.0.11) with parameters '-library-type fr-firststrand' and using Ensembl v.72 gene annotation. Mouse RNA-seq samples were aligned to mouse genome mm9 by Tophat (v. 2.0.11) with parameters '-library-type fr-firststrand' and using Ensembl version 67 gene annotation. The remaining downstream analysis steps are common to both human and mouse datasets.

Gene expression levels were quantified as the number of uniquely aligned reads overlapping with gene coordinates, using the feature counts function from Rsubread R package. Differentially expressed genes between conditions were identified using the DESeq2 R package and genes with Benjamini-Hochberg corrected P values < 0.05 were defined as differentially expressed. For PCA and unsupervised clustering, the read counts were normalized using rlog from DESeq2 (ref. ⁶⁶). Heatmaps were generated using the heatmap.2 function available in the gplots R package.

For GSEA, genes were ranked using 'Wald statistics' from DESeq2 results and GSEA was performed using GSEA desktop application v.2.2.7 with Molecular Signature Database v.3.1.

XCell⁴⁹ was used to infer the various cell types enriched in the samples; xCell uses gene signatures derived from 64 immune and stroma cell types to determine the cell-type composition in each sample. Normalized expression values (FPKM) were computed using R script and gene symbol, with the highest expression selected for duplicate gene symbols. Human homologues for mouse genes were retrieved using the MGI Human-Mouse homology report:

(www.informatics.jax.org/downloads/reports/HOM_MouseHumanSequence.rpt). Abundance scores were then computed using the xCell online version (<http://xcell.ucsf.edu/>) and visualized using boxplots.

Statistical analysis. GraphPad Prism v.8 was used for statistical analysis. Two-tailed, unpaired, Student's t -tests were used to estimate statistically significant differences between two groups. Two-way analysis of variance (ANOVA) with Tukey's post-hoc comparison was used for multiple comparisons. Values are presented as mean \pm s.d. unless otherwise indicated. Asterisks (*) always indicate significant differences as follows: NS, not significant, * $P < 0.05$, ** $P < 0.01$, *** $P < 0.001$.

For in vivo studies, mice were randomly assigned to treatment groups. All replicates in the present study represent different mice.

Reporting Summary. Further information on research design is available in the Reporting Summary linked to this article.

Data availability

The data that support the findings of this study are available from the corresponding author upon request. The RNA-seq data generated in the present study have been deposited in the Gene Expression Omnibus database under accession number [GSE122081](https://www.ncbi.nlm.nih.gov/geo/query/acc.cgi?acc=GSE122081). Source data for Figs. 1–6, Extended Data Figs. 1–9 and Supplementary Figs. 1, 2 and 4–7 are available online.

Received: 14 August 2019; Accepted: 10 September 2019;

Published online: 21 October 2019

References

- Kuifman, T., Michaloglou, C., Mooi, W. J. & Peeper, D. S. The essence of senescence. *Genes Dev.* **24**, 2463–2479 (2010).
- Herranz, N. & Gil, J. Mechanisms and functions of cellular senescence. *J. Clin. Invest.* **128**, 1238–1246 (2018).
- Salama, R., Sadaie, M., Hoare, M. & Narita, M. Cellular senescence and its effector programs. *Genes Dev.* **28**, 99–114 (2014).
- Coppe, J. P., Desprez, P. Y., Krtochka, A. & Campisi, J. The senescence-associated secretory phenotype: the dark side of tumor suppression. *Annu. Rev. Pathol.* **5**, 99–118 (2010).
- Kang, T. W. et al. Senescence surveillance of pre-malignant hepatocytes limits liver cancer development. *Nature* **479**, 547–551 (2011).
- Acosta, J. C. et al. A complex secretory program orchestrated by the inflammasome controls paracrine senescence. *Nat. Cell Biol.* **15**, 978–990 (2013).
- Tchkonia, T., Zhu, Y., van Deursen, J., Campisi, J. & Kirkland, J. L. Cellular senescence and the senescent secretory phenotype: therapeutic opportunities. *J. Clin. Invest.* **123**, 966–972 (2013).
- McHugh, D. & Gil, J. Senescence and aging: Causes, consequences, and therapeutic avenues. *J. Cell Biol.* **217**, 65–77 (2018).
- Munoz-Espin, D. & Serrano, M. Cellular senescence: from physiology to pathology. *Nat. Rev. Mol. Cell Biol.* **15**, 482–496 (2014).
- Baker, D. J. et al. Clearance of p16Ink4a-positive senescent cells delays ageing-associated disorders. *Nature* **479**, 232–236 (2011).
- Demaria, M. et al. An essential role for senescent cells in optimal wound healing through secretion of PDGF-AA. *Dev. Cell* **31**, 722–733 (2014).
- Baker, D. J. et al. Naturally occurring p16(Ink4a)-positive cells shorten healthy lifespan. *Nature* **530**, 184–189 (2016).
- Childs, B. G. et al. Senescent intimal foam cells are deleterious at all stages of atherosclerosis. *Science* **354**, 472–477 (2016).
- Jeon, O. H. et al. Local clearance of senescent cells attenuates the development of post-traumatic osteoarthritis and creates a pro-regenerative environment. *Nat. Med.* **23**, 775–781 (2017).
- Chinta, S. J. et al. Cellular senescence is induced by the environmental neurotoxin paraquat and contributes to neuropathology linked to Parkinson's disease. *Cell Rep.* **22**, 930–940 (2018).
- Bussian, T. J. et al. Clearance of senescent glial cells prevents tau-dependent pathology and cognitive decline. *Nature* **562**, 578–582 (2018).
- Zhu, Y. et al. The Achilles' heel of senescent cells: from transcriptome to senolytic drugs. *Aging Cell* **14**, 644–658 (2015).
- Wang, Y. et al. Discovery of piperlongumine as a potential novel lead for the development of senolytic agents. *Aging (Albany NY)* **8**, 2915–2926 (2016).
- Fuhrmann-Stroissnigg, H. et al. Identification of HSP90 inhibitors as a novel class of senolytics. *Nat. Commun.* **8**, 422 (2017).
- Chen, Q. et al. ABT-263 induces apoptosis and synergizes with chemotherapy by targeting stemness pathways in esophageal cancer. *Oncotarget* **6**, 25883–25896 (2015).
- Zhu, Y. et al. Identification of a novel senolytic agent, navitoclax, targeting the Bcl-2 family of anti-apoptotic factors. *Aging Cell* **15**, 428–435 (2016).
- Yosef, R. et al. Directed elimination of senescent cells by inhibition of BCL-W and BCL-XL. *Nat. Commun.* **7**, 11190 (2016).
- Ovadya, Y. & Krizhanovsky, V. Strategies targeting cellular senescence. *J. Clin. Invest.* **128**, 1247–1254 (2018).
- Georgilias, A. et al. PTBP1-mediated alternative splicing regulates the inflammatory secretome and the pro-tumorigenic effects of senescent cells. *Cancer Cell* **34**, 85–102 e109 (2018).
- Therien, A. G. & Blostein, R. Mechanisms of sodium pump regulation. *Am. J. Physiol. Cell Physiol.* **279**, C541–C566 (2000).
- Prassas, I. & Diamandis, E. P. Novel therapeutic applications of cardiac glycosides. *Nat. Rev. Drug Discov.* **7**, 926–935 (2008).
- Cheng, J. W. & Rybak, I. Use of digoxin for heart failure and atrial fibrillation in elderly patients. *Am. J. Geriatr. Pharmacother.* **8**, 419–427 (2010).
- Lopez-Lazaro, M. Digitoxin as an anticancer agent with selectivity for cancer cells: possible mechanisms involved. *Expert Opin. Ther. Targets* **11**, 1043–1053 (2007).
- Kurz, D. J., Decary, S., Hong, Y. & Erusalimsky, J. D. Senescence-associated (beta)-galactosidase reflects an increase in lysosomal mass during replicative ageing of human endothelial cells. *J. Cell Sci.* **113**, 3613–3622 (2000).
- Hildebrand, D. G. et al. alpha-Fucosidase as a novel convenient biomarker for cellular senescence. *Cell Cycle* **12**, 1922–1927 (2013).
- Dao, T. T. et al. Demethoxycurcumin is a potent inhibitor of P-Type ATPases from diverse kingdoms of life. *PLoS ONE* **11**, e0163260 (2016).
- Price, E. M. & Lingrel, J. B. Structure-function relationships in the Na,K-ATPase alpha subunit: site-directed mutagenesis of glutamine-111 to arginine and asparagine-122 to aspartic acid generates a ouabain-resistant enzyme. *Biochemistry* **27**, 8400–8408 (1988).
- Sieben, C. J., Sturmlechner, I., van de Sluis, B. & van Deursen, J. M. Two-step senescence-focused cancer therapies. *Trends Cell Biol.* **28**, 723–737 (2018).
- Collado, M. et al. Tumour biology: senescence in premalignant tumours. *Nature* **436**, 642 (2005).
- Michaloglou, C. et al. BRAFE600-associated senescence-like cell cycle arrest of human naevi. *Nature* **436**, 720–724 (2005).
- Braig, M. et al. Oncogene-induced senescence as an initial barrier in lymphoma development. *Nature* **436**, 660–665 (2005).
- Chen, Z. et al. Crucial role of p53-dependent cellular senescence in suppression of Pten-deficient tumorigenesis. *Nature* **436**, 725–730 (2005).
- Gonzalez-Meljem, J. M. et al. Stem cell senescence drives age-attenuated induction of pituitary tumours in mouse models of paediatric craniopharyngioma. *Nat. Commun.* **8**, 1819 (2017).
- Gaston-Massuet, C. et al. Increased Wingless (Wnt) signaling in pituitary progenitor/stem cells gives rise to pituitary tumors in mice and humans. *Proc. Natl Acad. Sci. USA* **108**, 11482–11487 (2011).
- Schmitt, C. A. et al. A senescence program controlled by p53 and p16INK4a contributes to the outcome of cancer therapy. *Cell* **109**, 335–346 (2002).

41. Demaria, M. et al. Cellular senescence promotes adverse effects of chemotherapy and cancer relapse. *Cancer Discov.* **7**, 165–176 (2016).
42. Wang, L. et al. High-throughput functional genetic and compound screens identify targets for senescence induction in cancer. *Cell Rep.* **21**, 773–783 (2017).
43. Wang, L. & Bernards, R. Taking advantage of drug resistance, a new approach in the war on cancer. *Front. Med.* **12**, 490–495 (2018).
44. Rudalska, R. et al. In vivo RNAi screening identifies a mechanism of sorafenib resistance in liver cancer. *Nat. Med.* **20**, 1138–1146 (2014).
45. Chang, J. et al. Clearance of senescent cells by ABT263 rejuvenates aged hematopoietic stem cells in mice. *Nat. Med.* **22**, 78–83 (2016).
46. Childs, B. G., Durik, M., Baker, D. J. & van Deursen, J. M. Cellular senescence in aging and age-related disease: from mechanisms to therapy. *Nat. Med.* **21**, 1424–1435 (2015).
47. Selden, R. & Smith, T. W. Ouabain pharmacokinetics in dog and man. Determination by radioimmunoassay. *Circulation* **45**, 1176–1182 (1972).
48. Salive, M. E. et al. Serum albumin in older persons: relationship with age and health status. *J. Clin. Epidemiol.* **45**, 213–221 (1992).
49. Aran, D., Hu, Z. & Butte, A. J. xCell: digitally portraying the tissue cellular heterogeneity landscape. *Genome Biol.* **18**, 220 (2017).
50. Wilson, W. H. et al. Navitoclax, a targeted high-affinity inhibitor of BCL-2, in lymphoid malignancies: a phase 1 dose-escalation study of safety, pharmacokinetics, pharmacodynamics, and antitumour activity. *Lancet Oncol.* **11**, 1149–1159 (2010).
51. Childs, B. G. et al. Senescent cells: an emerging target for diseases of ageing. *Nat. Rev. Drug Discov.* **16**, 718–735 (2017).
52. Triana-Martinez, F. et al. Identification and characterization of cardiac glycosides as senolytic compounds. *Nat. Commun.* <https://doi.org/10.1038/s41467-019-12888-x> (2019).
53. Mijatovic, T. et al. Cardiotonic steroids on the road to anti-cancer therapy. *Biochim. Biophys. Acta* **1776**, 32–57 (2007).
54. Menger, L. et al. Cardiac glycosides exert anticancer effects by inducing immunogenic cell death. *Sci. Transl. Med.* **4**, 143ra199 (2012).
55. Shi, H. et al. Digoxin reduces atherosclerosis in apolipoprotein E-deficient mice. *Br. J. Pharm.* **173**, 1517–1528 (2016).
56. Li, B. et al. Ouabain ameliorates bleomycin induced pulmonary fibrosis by inhibiting proliferation and promoting apoptosis of lung fibroblasts. *Am. J. Transl. Res.* **10**, 2967–2974 (2018).
57. Whayne, T. F. Jr. Clinical use of digitalis: a state of the art review. *Am. J. Cardiovasc. Drugs* **18**, 427–440 (2018).
58. Banito, A. et al. Senescence impairs successful reprogramming to pluripotent stem cells. *Genes Dev.* **23**, 2134–2139 (2009).
59. Barradas, M. et al. Histone demethylase JMJD3 contributes to epigenetic control of INK4a/ARF by oncogenic RAS. *Genes Dev.* **23**, 1177–1182 (2009).
60. Agostini, S. et al. Inhibition of non canonical HIV-1 Tat secretion through the cellular Na⁺,K⁺-ATPase blocks HIV-1 infection. *EBioMedicine* **21**, 170–181 (2017).
61. Fellmann, C. et al. An optimized microRNA backbone for effective single-copy RNAi. *Cell Rep.* **5**, 1704–1713 (2013).
62. Tordella, L. et al. SWI/SNF regulates a transcriptional program that induces senescence to prevent liver cancer. *Genes Dev.* **30**, 2187–2198 (2016).
63. Herranz, N. et al. mTOR regulates MAPKAPK2 translation to control the senescence-associated secretory phenotype. *Nat. Cell Biol.* **17**, 1205–1217 (2015).
64. Andoniadou, C. L. et al. Lack of the murine homeobox gene *Hesx1* leads to a posterior transformation of the anterior forebrain. *Development* **134**, 1499–1508 (2007).
65. Harada, N. et al. Intestinal polyposis in mice with a dominant stable mutation of the beta-catenin gene. *EMBO J.* **18**, 5931–5942 (1999).
66. Love, M. I., Huber, W. & Anders, S. Moderated estimation of fold change and dispersion for RNA-seq data with DESeq2. *Genome Biol.* **15**, 550 (2014).

Acknowledgements

We are grateful to members of J. Gil's laboratory for reagents, comments and other contributions to this project. We thank R. Laberge and A. Bhushan for feedback and members of the Genomics LMS facility (L. Game, K. Rekopoulou and A. Ivan) for help with RNA-seq. Core support from Medical Research Council (MRC; MC_U120085810) and grants from Worldwide Cancer Research (WCR; 18-0215), LifeArc and Unity Biotechnology funded this research in J. Gil's laboratory. D.J.W. was funded by a Wellcome Trust Strategic Award (no. 098565) and core support from the MRC (MC-A654-5QB40). L.Z. is supported by the German Research Foundation: DFG EXC 2180-390900677 ('Image Guided and Functionally Instructed Tumour Therapies'); FOR2314, SFB-TR209, Gottfried Wilhelm Leibniz Program; the German Ministry for Education and Research: eMed/Multiscale HCC; the European Research Council: Concolidartor grant 'CholangioConcept'; and the German Centre for Translational Cancer Research. J.P.M.-B. was funded by the Brain Tumour Charity (SIGNAL and EVEREST), Great Ormond Street Hospital (GOSH) Children's Charity and the National Institute of Health Research Biomedical Research Centre at GOSH for Children NHS Foundation Trust and University College London. J.P.M.-B. is a GOSH for Children's Charity Principal Investigator. S.M. is a PhD fellow funded by Boehringer Ingelheim Fonds.

Author contributions

A.G. and N.H. performed, designed and analysed the experiments, and wrote the manuscript. B.S., V.W., A.J.I., J. Birch, J.H., A.O., S.G., R.G., K.W., J.P., E.E.I., D.H., J. Glegola and S.M. performed, designed and analysed the experiments. G.D. carried out the bioinformatics analysis. J. Behmoaras, D.D., A.G.U., L.Z., S.V., J.P.M.-B. and D.J.W. designed the experiments and secured funding. J. Gil conceived and designed the project, secured funding and wrote the manuscript, with all authors providing feedback.

Competing interests

J. Gil owns equity and has acted as a consultant for Unity Biotechnology and Geras Bio. Unity Biotechnology funded research on senolytics in J. Gil's laboratory. J. Gil, A.G. and N.H. are named inventors in an MRC patent related to senolytic therapies (PCT/GB2018/051437).

Additional information

Extended data is available for this paper at <https://doi.org/10.1038/s42255-019-0122-z>.

Supplementary information is available for this paper at <https://doi.org/10.1038/s42255-019-0122-z>.

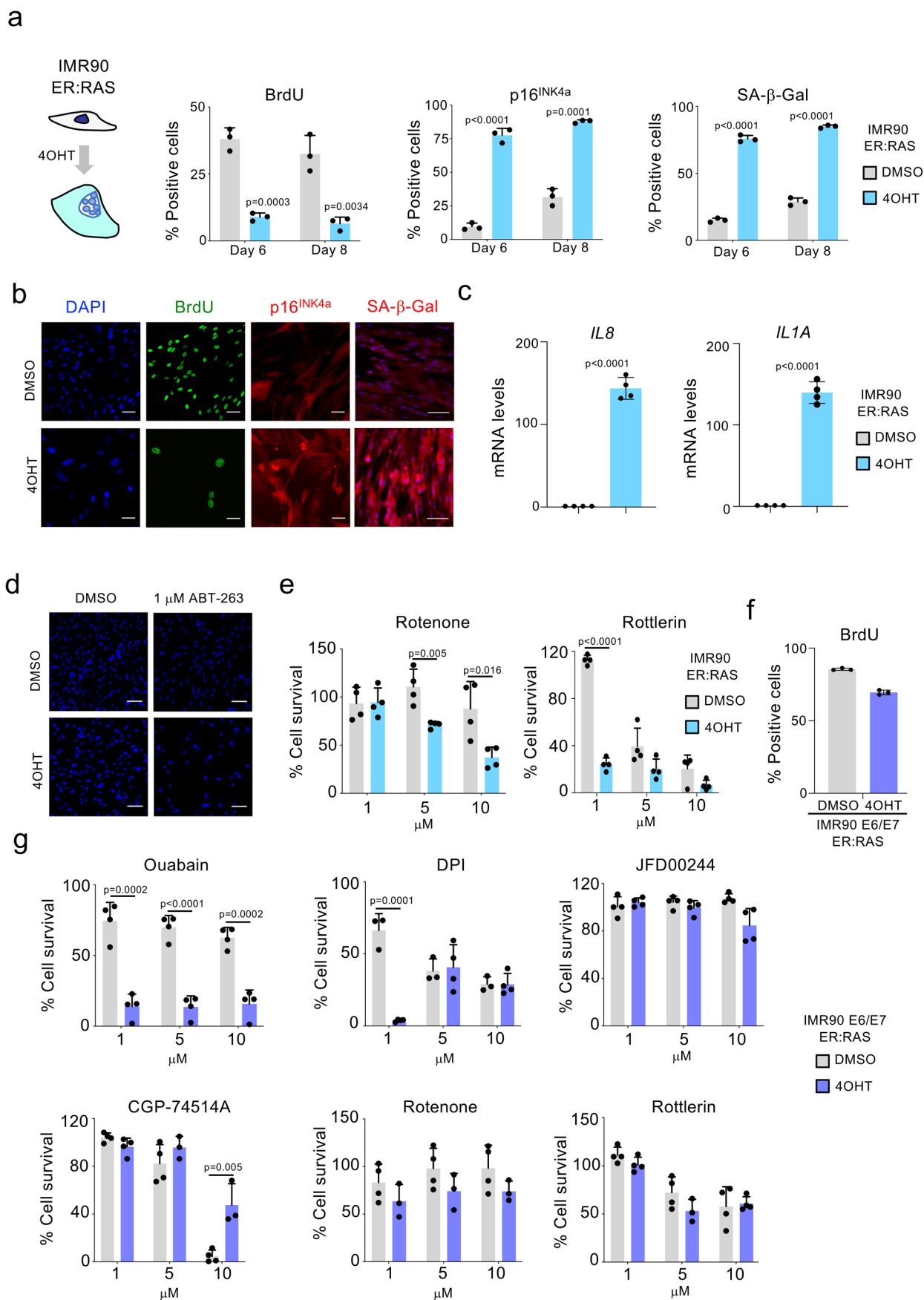
Correspondence and requests for materials should be addressed to J. Gil.

Peer review information Primary Handling Editor: Christoph Schmitt.

Reprints and permissions information is available at www.nature.com/reprints.

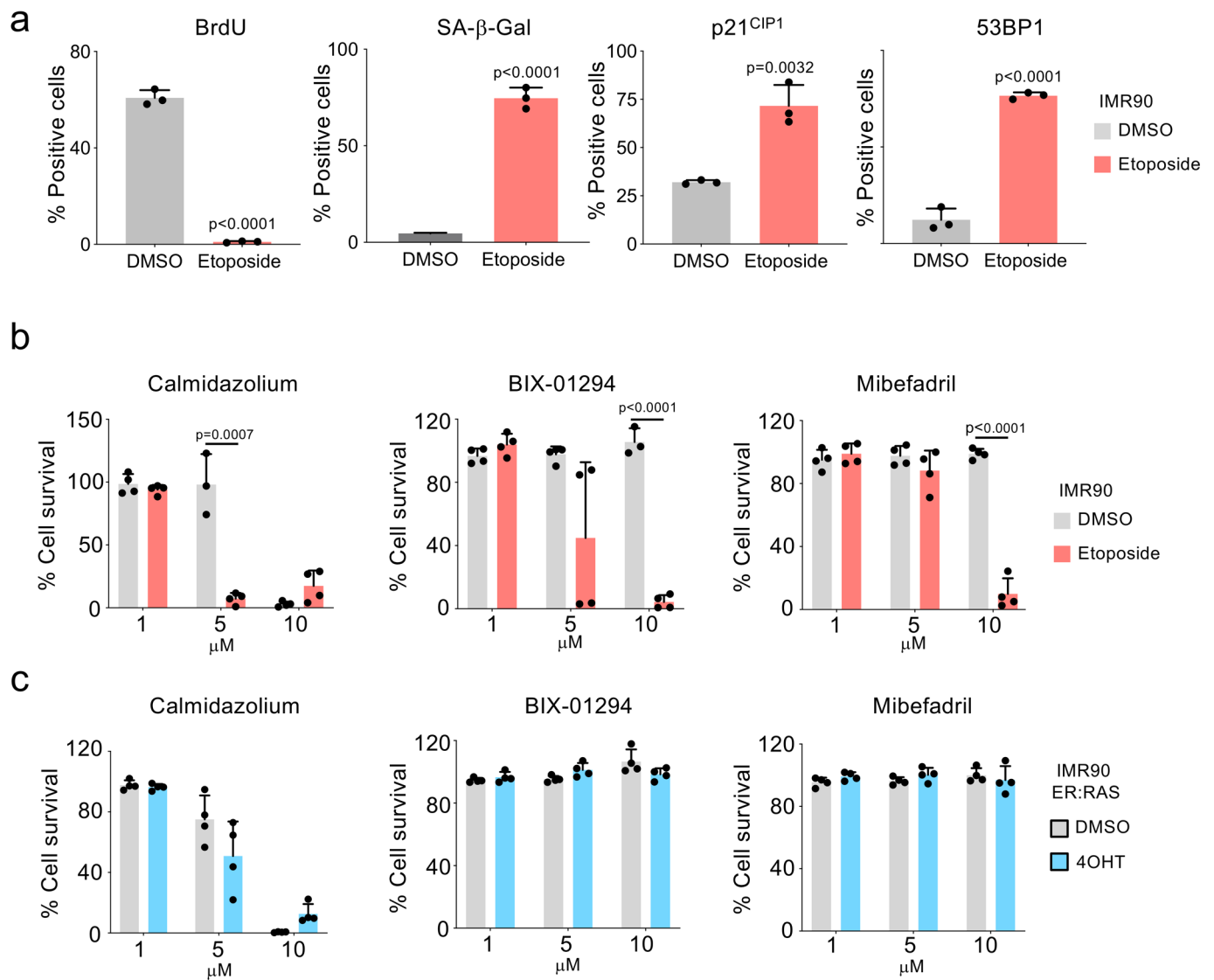
Publisher's note Springer Nature remains neutral with regard to jurisdictional claims in published maps and institutional affiliations.

© The Author(s), under exclusive licence to Springer Nature Limited 2019

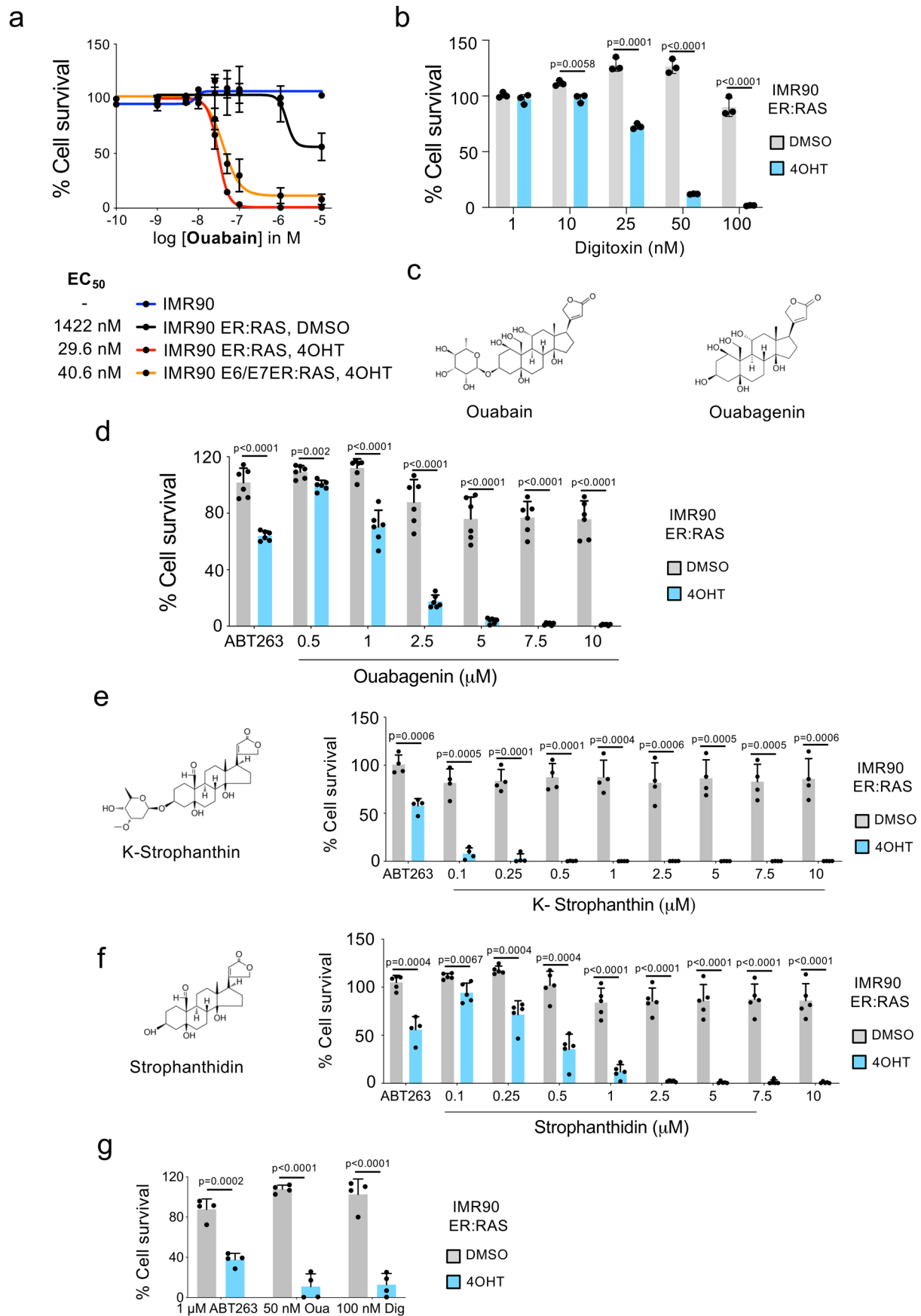


Extended Data Fig. 1 | see figure caption on next page.

Extended Data Fig. 1 | IMR90 ER:RAS cells as a model of OIS. **a**, Quantification of immunofluorescence staining for BrdU, p16^{INK4a}, and SA- β -Galactosidase of IMR90 ER:RAS cells 6 or 8 days after treatment with 4-OHT or vehicle (DMSO) ($n = 3$). **b**, Representative immunofluorescence images. BrdU incorporation, which indicates proliferation, is stained green; p16^{INK4a} is stained red. Scale bar, 50 μ m. SA- β -Galactosidase is stained red. Scale bar, 100 μ m. **c**, Expression levels for *IL8* and *IL1A* of senescent and control IMR90 ER:RAS cells 6 days after 4-OHT or vehicle (DMSO) ($n = 4$). **d**, DAPI staining of senescent and control IMR90 ER:RAS cells after 1 μ M ABT-263 treatment for 3 days showing reduced numbers of senescent cells after ABT-263 treatment. Scale bar, 100 μ m. **e**, Senolytic activity of the indicated drugs in the context of oncogene-induced senescence in IMR90 ER:RAS cells ($n = 4$). **f**, Quantification of immunofluorescence staining for BrdU in IMR90 ER:RAS cells expressing E6 and E7 proteins of HPV16 ($n = 3$). **g**, Senolytic activity of the indicated drugs in IMR90 ER:RAS cells expressing E6 and E7 proteins of HPV16. All error bars represent mean \pm s.d; n represents independent experiments. All statistical significances were calculated using unpaired two-tailed Student's *t*-tests.

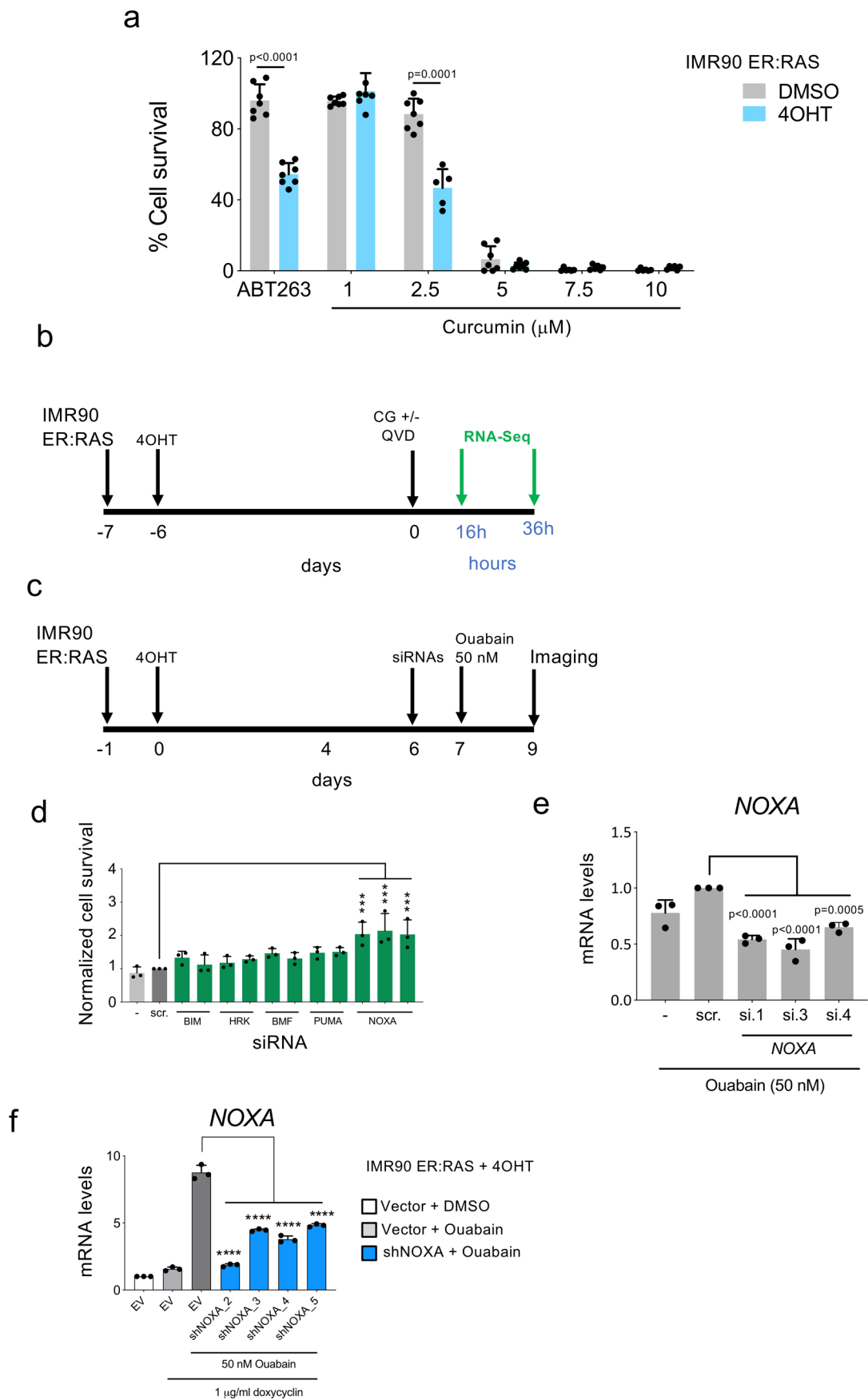


Extended Data Fig. 2 | Senolytic drug screen in therapy-induced senescence. **a**, Quantification of immunofluorescence staining for BrdU, SA-β-Galactosidase activity, p21^{CIP1} and 53BP1 in IMR90 cells treated with 50 μM etoposide ($n = 3$). **b-c**, Senolytic activity of the indicated drugs in the context of therapy-induced senescence in IMR90 ($n = 4$, **b**) and oncogene-induced senescence in IMR90 ER:RAS cells ($n = 4$, **c**). All error bars represent mean \pm s.d; n represents independent experiments. All statistical significances were calculated using unpaired two-tailed Student's t -tests.



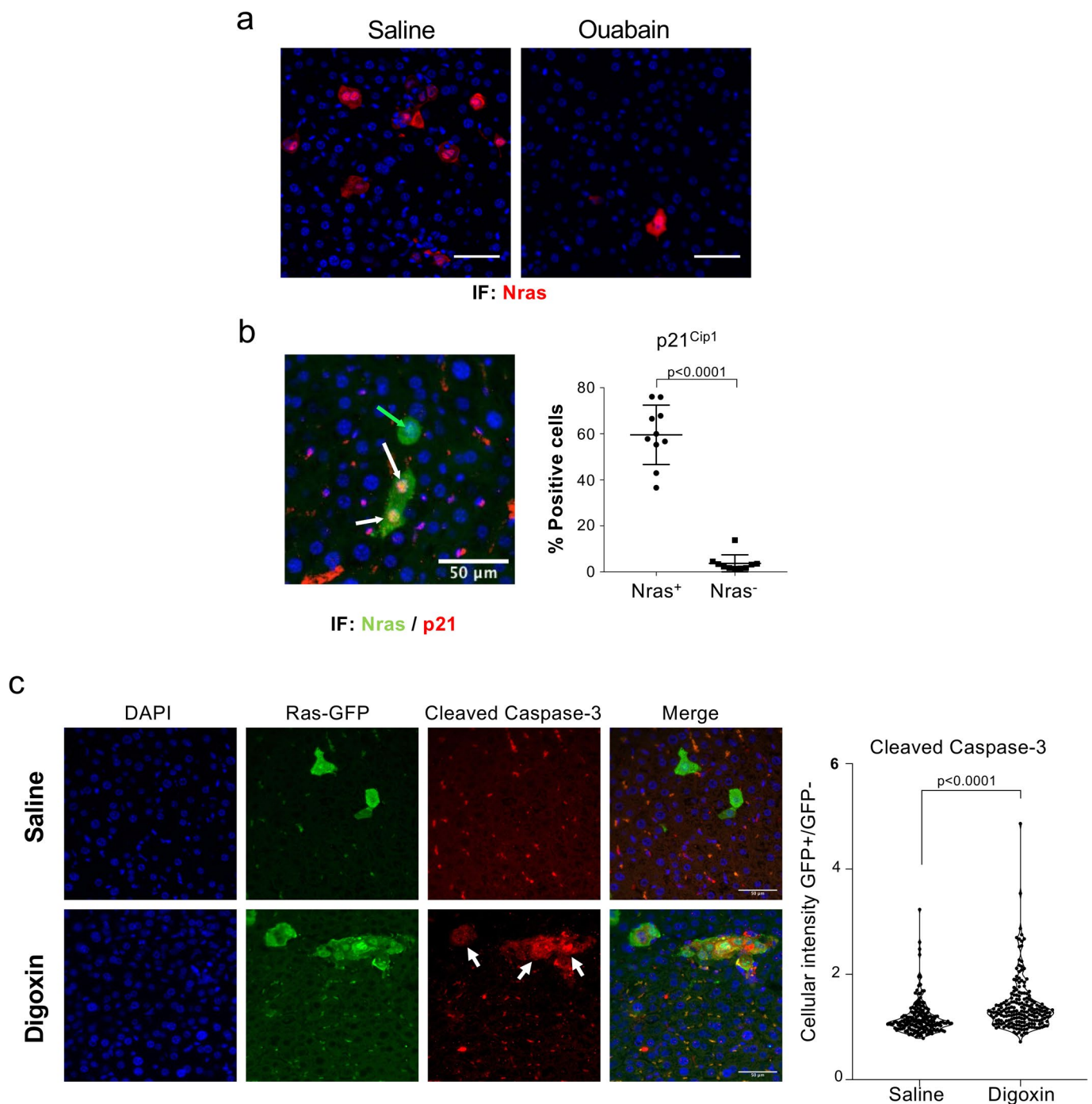
Extended Data Fig. 3 | see figure caption on next page.

Extended Data Fig. 3 | The glycoside chain in CGs is dispensable for their senolytic activity. **a**, Dose response analysis of senolytic activity of ouabain in IMR90, control IMR90 ER:RAS cells (DMSO), senescent IMR90 ER:RAS cells (4-OHT) and IMR90 ER:RAS cells expressing E6 and E7 proteins of HPV16 ($n = 3$). **b**, Dose response analysis of senolytic activity of digitoxin in the context of oncogene-induced senescence in IMR90 ER:RAS cells ($n = 3$). **c**, Chemical structure of ouabain and its aglycone version, ouabagenin. **d**, Quantification of cell survival in senescent and control IMR90 ER:RAS cells after treatment with ouabagenin, the aglycone version of ouabain ($n = 6$). **e-f**, Quantification of cell survival of IMR90 ER:RAS cells undergoing OIS and the corresponding controls after treatment with the CG K-Strophanthin (**e**) ($n = 4$) or its aglycone version Strophanthidin (**f**) ($n = 5$). **g**, Quantification of cell survival in senescent and control IMR90 ER:RAS 3 days after 1 μM ABT-263 or treatment with CGs (50 nM ouabain, 100 nM digoxin). Senolytic drugs were added 8 days after 4-OHT or vehicle (DMSO) ($n = 4$). All error bars represent mean \pm s.d.; n represents independent experiments. All statistical significances were calculated using unpaired two-tailed Student's t -tests.

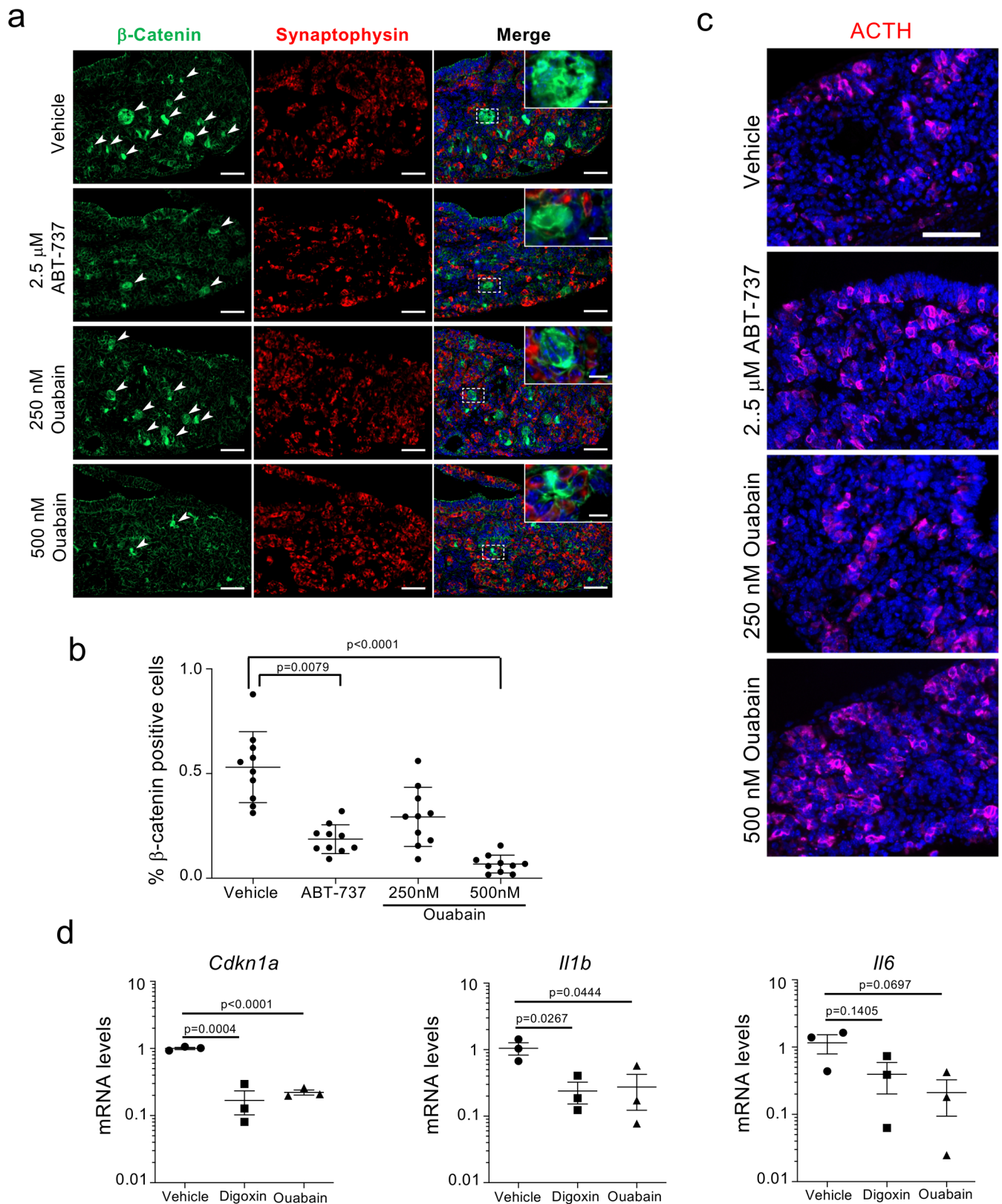


Extended Data Fig. 4 | see figure caption on next page.

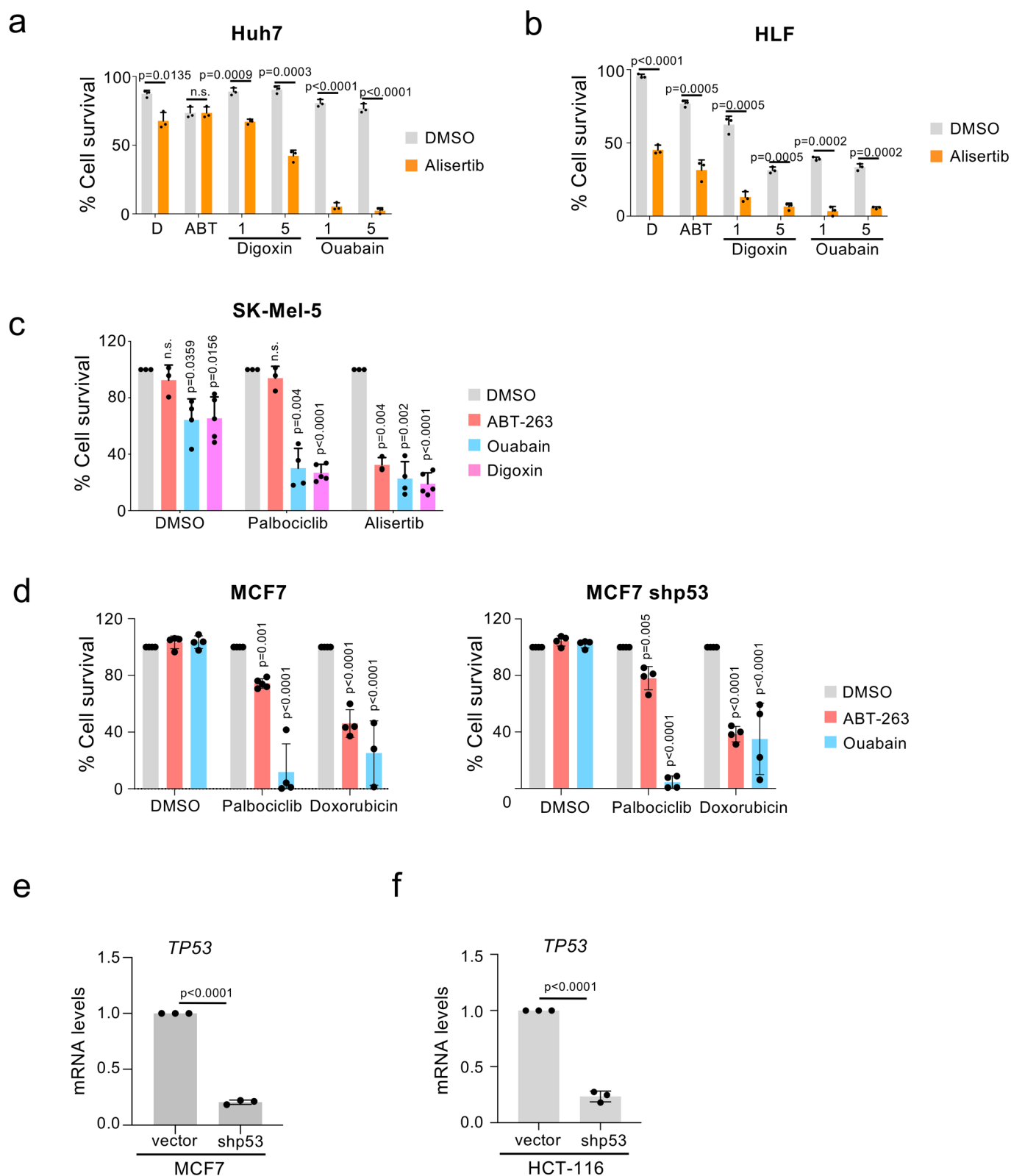
Extended Data Fig. 4 | Senescent cells are more sensitive to CGs due to their altered osmotic balance. **a**, Quantification of cell survival of senescent and control IMR90 ER:RAS cells after treatment with curcumin ($n = 6$). Statistical significance was calculated using unpaired two-tailed, Student's *t*-test. **b**, Experimental design for the transcriptional profiling of senescent and control IMR90 ER:RAS cells after treatment with cardiac glycosides (CGs). QVD indicates treatment with a general caspase inhibitor (Q-VD-OPh). **c**, IMR90 ER:RAS cells were transfected with 2 independent siRNAs targeting *BCL-2* family genes at day 6 after senescence induction as indicated in the scheme. **d**, IMR90 ER:RAS were transfected with at least two independent siRNAs targeting *BCL-2* family genes at day 6 after senescence induction ($n = 3$; scrambled siRNA versus three different siRNAs against *NOXA*, $***P < 0.001$). The timeline of the experiment is shown in **(c)**. Statistical significance was calculated using one-way ANOVA (Dunnett's test). **e**, Expression levels of *NOXA* after knock down with three independent siRNAs ($n = 3$). Statistical significance was calculated using one-way ANOVA (Dunnett's test). **f**, Expression levels of *NOXA* after knock down with four independent shRNAs ($n = 3$; vector versus different shRNAs against *NOXA*, $****P < 0.0001$). Statistical significance was calculated using one-way ANOVA (Dunnett's test). All error bars represent mean \pm s.d; *n* represents independent experiments.



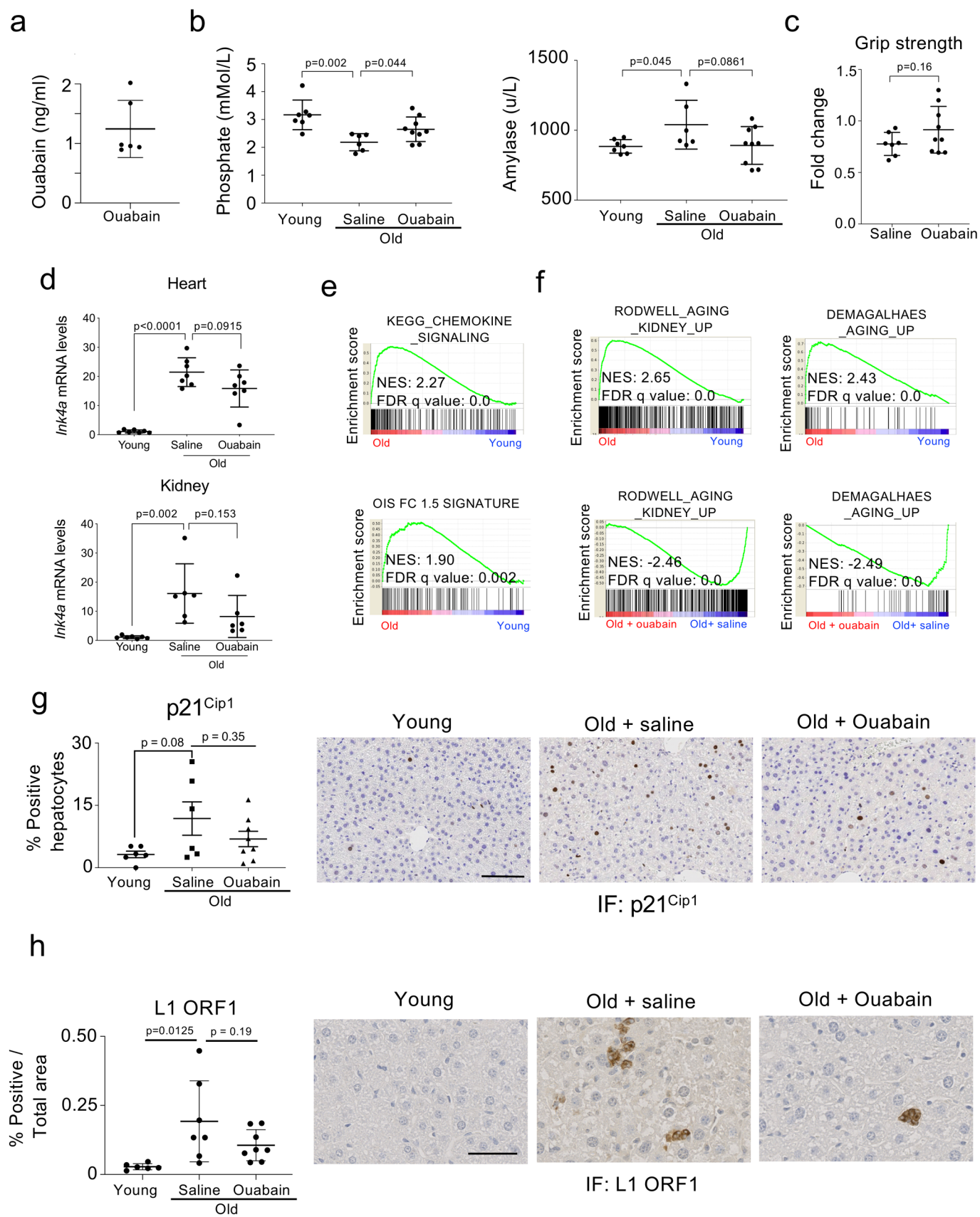
Extended Data Fig. 5 | Ouabain eliminates liver preneoplastic senescent cells. **a**, Representative images of immunofluorescence staining of Nras. Mice were treated with vehicle ($n = 9$) or ouabain ($n = 12$) as explained in Fig 4a. Nras is stained in red. Scale bar, 70 μm . **b**, Immunofluorescence staining and quantification of p21^{Cip1} in Nras-positive senescent hepatocytes vs Nras-negative normal hepatocytes. Nras is stained in green, p21^{Cip1} is stained in red. White arrows indicate Nras-positive, p21^{Cip1}-positive cells; green arrow indicates a Nras-positive, p21^{Cip1}-negative cells ($n = 10$ per group). **c**, SCID/beige mice were treated with saline or Digoxin (1mg/kg) on two consecutive days, 5 days after hydrodynamic transduction of Nras-GFP. Mice were culled 6 hours after the second treatment. Representative images of immunofluorescence staining of GFP and cleaved caspase-3 and quantification of intensity levels in 1/2 independent experiments ($n = 200$ cells). Scale bar, 50 μm . Statistical significance was calculated using unpaired two-tailed Student's t-test. Data represent mean \pm s.d.; n represents number of mice.



Extended Data Fig. 6 | Ouabain eliminates preneoplastic senescent cells. **a**, Representative images of immunofluorescence staining of β -catenin (green) and synaptophysin (red) in tumoral pituitaries from 18.5 dpc *Hesx1^{Cre/+};Ctnnb1^{lox(ex3)/+}* mice that were cultured in the presence of either ABT-737 (2.5 μ M), ouabain (250 nM and 500 nM) or vehicle (DMSO) ($n = 10$ per group). Scale bar, 50 μ m. **b**, Quantitative analysis of the immunofluorescence in **(a)** demonstrates that ABT-737 and ouabain significantly reduce the number of β -catenin-positive cells. Statistical significance was calculated using Kruskal-Wallis and Dunn's multiple comparisons test. **c**, Representative images of immunofluorescence staining of ACTH (adrenocorticotrophic hormone; magenta). Scale bar: 50 μ m. **d**, qRT-PCR analysis revealing that the senescent marker *Cdkn1a* (encoding for p21^{Cip1}) and the SASP components *Il1b* and *Il6* are reduced in neoplastic pituitaries treated with 100 nM ouabain and 100 nM digoxin relative to vehicle controls ($n = 3$ per group). Statistical significance was calculated using unpaired two-tailed Student's t-test; data represent mean \pm s.d.; n represents number of mice.

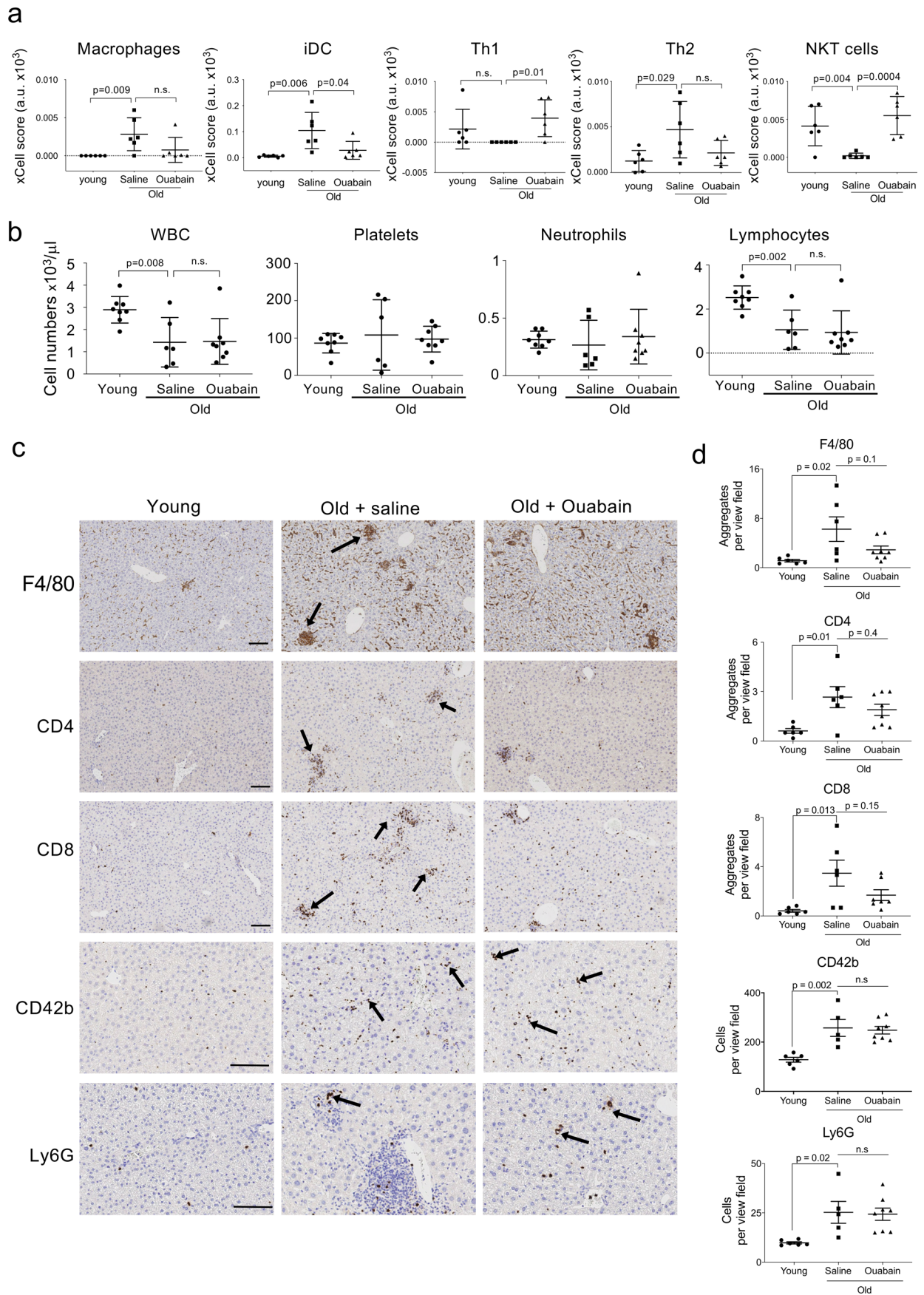


Extended Data Fig. 7 | Anti-cancer effect of cardiac glycosides across different human cancer cell lines. a–b, Quantification of cell survival by trypan blue staining of Huh7 cells (**a**) and HLF cells (**b**) after treatment with the indicated drug combinations ($n = 3$). Timeline of the experiment is shown in Supplementary Fig 4a. Statistical significance was calculated using unpaired two-tailed Student's *t*-test. **c,** Quantification of cell survival of senescent (alisertib, palbociclib) and control (DMSO) SK-Mel-5 melanoma cells ($n = 4$). Statistical significance was calculated using two-way ANOVA (Dunnett's test). **d,** Quantification of cell survival of senescent (doxorubicin, palbociclib) and control (DMSO) MCF7 or MCF7 breast cancer cells infected with a shRNA against *TP53* ($n = 4$). Statistical significance was calculated using two-way ANOVA (Dunnett's test). **e–f,** mRNA expression levels of *TP53* in MCF7 cells (**e**) and HCT116 cells ($n = 3$). Statistical significance was calculated using unpaired two-tailed, Student's *t*-test. Data represent mean \pm s.d.; *n* represents independent experiments; ns, not significant.



Extended Data Fig. 8 | see figure caption on next page.

Extended Data Fig. 8 | Ouabain treatment reverses age-associated changes in old mice. **a**, Ouabain levels in plasma were assessed by ELISA 24 hours after finishing a 4-day course of daily 1mg/kg ouabain i.p. injections. ($n = 6$). **b**, Phosphate and amylase levels of young ($n = 7$) and old mice, either treated with vehicle ($n = 6$) or ouabain ($n = 9$), were determined in whole-blood samples at the endpoint of the experiment. Statistical significance was calculated using unpaired two-tailed Student's *t*-test. **c**, Grip strength assessment in old mice treated with vehicle ($n = 7$) or ouabain ($n = 9$) 10 weeks after the start of the experiment, referred to the basal test. Statistical significance was calculated using unpaired two-tailed Student's *t*-test. **d**, Expression levels of *p16^{INK4a}* in heart and kidney were determined by qRT-PCR following treatment with vehicle ($n = 6$) or ouabain ($n = 7$). mRNA expression levels in young mice ($n = 7$) were used as reference. Statistical significance was calculated using unpaired two-tailed Student's *t*-test. **e-f**, GSEA signature for chemokines, oncogene-induced senescence (**e**) and ageing (**f**). **g**, Quantitative analysis (left) and representative IHC pictures (right) of p21^{CIP1} positive hepatocytes in the liver of young ($n = 6$) and old mice treated with ouabain ($n = 8$) or vehicle (saline) ($n = 6$). Scale bar, 100 μm . Data represent mean \pm s.e.m. Statistical significance was calculated using one-way ANOVA with Tukey's post hoc comparison. **h**, Quantitative analysis (left) and representative IHC pictures (right) of LINE-1 ORF in the liver of young ($n = 6$) and old mice treated with ouabain ($n = 8$) or vehicle (saline) ($n = 7$). Statistical significance was calculated using one-way ANOVA with Tukey's post hoc comparison. Scale bar, 50 μm . Data represent mean \pm s.d; *n* represents number of mice.



Extended Data Fig. 9 | see figure caption on next page.

Extended Data Fig. 9 | Ouabain treatment resets immune infiltration in old mice. **a**, xCell analysis of the transcriptome data predicts changes in immune infiltration in the liver of old mice that could be reverted with ouabain. RNA-Seq data from the livers of young ($n = 6$) and old mice, either treated with vehicle ($n = 6$) or ouabain ($n = 6$) was used. Statistical significance was calculated using unpaired two-tailed Student's t -test. **b**, Blood analysis at the end of the experiment show that ouabain treatment does not change immune composition. Blood from young ($n = 8$) and old mice, either treated with vehicle ($n = 6$) or ouabain ($n = 8$) was used. Statistical significance was calculated using unpaired two-tailed Student's t -test. **c-d**, Representative IHC images (**c**) and quantification (**d**) of the indicated immune cell markers in the liver of young ($n = 6$) and old mice, either treated with vehicle ($n = 6$) or ouabain ($n = 8$). Scale bar: 100 μ m. Statistical significance was calculated using one-way ANOVA with Tukey's post hoc comparison. Data represent mean \pm s.e.m.; n represents number of mice; ns, not significant.

Reporting Summary

Nature Research wishes to improve the reproducibility of the work that we publish. This form provides structure for consistency and transparency in reporting. For further information on Nature Research policies, see [Authors & Referees](#) and the [Editorial Policy Checklist](#).

Statistics

For all statistical analyses, confirm that the following items are present in the figure legend, table legend, main text, or Methods section.

n/a Confirmed

- The exact sample size (n) for each experimental group/condition, given as a discrete number and unit of measurement
- A statement on whether measurements were taken from distinct samples or whether the same sample was measured repeatedly
- The statistical test(s) used AND whether they are one- or two-sided
Only common tests should be described solely by name; describe more complex techniques in the Methods section.
- A description of all covariates tested
- A description of any assumptions or corrections, such as tests of normality and adjustment for multiple comparisons
- A full description of the statistical parameters including central tendency (e.g. means) or other basic estimates (e.g. regression coefficient) AND variation (e.g. standard deviation) or associated estimates of uncertainty (e.g. confidence intervals)
- For null hypothesis testing, the test statistic (e.g. F , t , r) with confidence intervals, effect sizes, degrees of freedom and P value noted
Give P values as exact values whenever suitable.
- For Bayesian analysis, information on the choice of priors and Markov chain Monte Carlo settings
- For hierarchical and complex designs, identification of the appropriate level for tests and full reporting of outcomes
- Estimates of effect sizes (e.g. Cohen's d , Pearson's r), indicating how they were calculated

Our web collection on [statistics for biologists](#) contains articles on many of the points above.

Software and code

Policy information about [availability of computer code](#)

Data collection

IN Cell Analyzer 2000 version 5.2-14311 (64-bit) GE Healthcare.
IncuCyte ZOOM 2018A (2018.1.6628.28170).
Microsoft Excel 2016 16.16.13 (190811).

Data analysis

GraphPad Prism 8 (version 8.1.2) for macOS High Sierra was used for statistical analysis.
IN Cell Investigator 1000 workstation 3.7.2, build 1860.
ImageJ 2.0.0-rc-54/1.51g.
FASTQC 0.11.5
Tophat (v 2.0.11).
Ensembl version 72 and version 67 gene annotation.
Rsubread R package. 1.28.1
DESeq2 R package 1.18.1
heatmap.2 in gplots R package. 3.0.1
GSEA desktop application version 2.2.7 with Molecular Signature database version 3.1.
xCell, web based: <http://xCell.ucsf.edu/>

For manuscripts utilizing custom algorithms or software that are central to the research but not yet described in published literature, software must be made available to editors/reviewers. We strongly encourage code deposition in a community repository (e.g. GitHub). See the Nature Research [guidelines for submitting code & software](#) for further information.

Data

Policy information about [availability of data](#)

All manuscripts must include a [data availability statement](#). This statement should provide the following information, where applicable:

- Accession codes, unique identifiers, or web links for publicly available datasets
- A list of figures that have associated raw data
- A description of any restrictions on data availability

The data that supports the findings of this study are available from the corresponding author upon request. The RNA-seq data generated in this study have been deposited in the GEO database under accession number GSE122081 and can be accessed using the token sbydiscusdlsjyff on the following private link: <https://www.ncbi.nlm.nih.gov/geo/query/acc.cgi?acc=GSE122081>

Field-specific reporting

Please select the one below that is the best fit for your research. If you are not sure, read the appropriate sections before making your selection.

- Life sciences Behavioural & social sciences Ecological, evolutionary & environmental sciences

For a reference copy of the document with all sections, see [nature.com/documents/nr-reporting-summary-flat.pdf](https://www.nature.com/documents/nr-reporting-summary-flat.pdf)

Life sciences study design

All studies must disclose on these points even when the disclosure is negative.

Sample size	Sample size was not predetermined. Generally accepted samples sizes were used, with reproducible differences between conditions indicating that sample size is sufficient.
Data exclusions	All data were included.
Replication	All experiments were reproducible. Every figure states how many times each experiment was performed with similar results.
Randomization	For animal experiments, littermates were randomly allocated to treatment groups. Cell culture experiments are normally not randomized.
Blinding	Investigators were blinded for the evaluation of histological sections. Investigators were not blinded for analysis relying on unbiased measurements of quantitative parameters.

Reporting for specific materials, systems and methods

We require information from authors about some types of materials, experimental systems and methods used in many studies. Here, indicate whether each material, system or method listed is relevant to your study. If you are not sure if a list item applies to your research, read the appropriate section before selecting a response.

Materials & experimental systems

n/a	Involved in the study
<input type="checkbox"/>	<input checked="" type="checkbox"/> Antibodies
<input type="checkbox"/>	<input checked="" type="checkbox"/> Eukaryotic cell lines
<input checked="" type="checkbox"/>	<input type="checkbox"/> Palaeontology
<input type="checkbox"/>	<input checked="" type="checkbox"/> Animals and other organisms
<input checked="" type="checkbox"/>	<input type="checkbox"/> Human research participants
<input checked="" type="checkbox"/>	<input type="checkbox"/> Clinical data

Methods

n/a	Involved in the study
<input checked="" type="checkbox"/>	<input type="checkbox"/> ChIP-seq
<input checked="" type="checkbox"/>	<input type="checkbox"/> Flow cytometry
<input checked="" type="checkbox"/>	<input type="checkbox"/> MRI-based neuroimaging

Antibodies

Antibodies used

The following primary antibodies were used in this study: mouse monoclonal anti-BrdU (3D4; BD Biosciences, 555627) 1:2000, rabbit polyclonal anti-GAPDH (Abcam, ab225555) 1:2500, mouse monoclonal anti-p16INK4a (JC-8; from CRUK) 1:1000, rabbit polyclonal anti-p21 (M-19; Santa Cruz, sc-471) 1:200, rabbit monoclonal anti-phospho-c-Jun (Ser73; D47G9, Cell Signaling Technology, 3270) 1:1500, rabbit monoclonal anti-phospho-GSK-3 β (Ser9; D85E12, Cell Signaling Technology, 5558) 1:2000, rabbit polyclonal anti-phospho-Akt (Ser473; Cell Signaling Technology, 9271) 1:2000, rabbit polyclonal anti-phospho-p38 MAPK (Thr180/Tyr182; Cell Signaling Technology, 9211) 1:2000, rabbit polyclonal anti- β -Catenin (Thermo, RB-9035-P1) 1:500, mouse monoclonal anti-ACTH (Fitzgerald, N/A) 1:1000, mouse polyclonal anti-p21 (BD Biosciences, 556431) 1:200, mouse monoclonal anti-Synaptophysin (27G12; Leica, NCL-L-SYNAP-299) 1:250, rat anti-MHCII (M5/114.15.2; Novus Biologicals, NBP1-43312) 1:500, rabbit polyclonal anti-CD68 (Abcam, ab125212) 1:100, rabbit monoclonal anti-CD3 (SP7; Zytomed, RBK024) 1:250, rat monoclonal anti-B220 (BD Biosciences, 553084) 1:3000, rat monoclonal anti-F4/80 (Linaris, T2006) 1:120, rat monoclonal anti-

Validation

CD4 (eBioscience, 14-9766) 1:1000, mouse monoclonal anti-N-Ras (F155, Santa Cruz, sc-31), rabbit monoclonal anti-cleaved caspase 3 (Asp175; 5A1E; Cell Signaling Technology, 9664) 1:400, rabbit monoclonal anti-LINE-1 ORF1p (EPR21844-108; Abcam, ab216324) 1:500, rat monoclonal anti-CD8alpha (Invitrogen, 14-0808-82) 1:200, rabbit monoclonal anti-CD42b (Abcam, ab183345) 1:200, rat Ly-6g (BD Biosciences, 551459) 1:800, rabbit polyclonal anti-GLB1 (Proteintech, 15518-1AP) 1:100, rabbit monoclonal anti- Ki67 (Abcam, ab16667) 1:100, rat monoclonal anti-GFP (3H9, Chromotek) 1:200.
We used the following secondary antibodies: goat anti-mouse IgG (H+L, AlexaFluor 488 conjugated, Thermo Fischer Scientific, A11029), goat anti-mouse IgG (H+L), AlexaFluor 594 conjugated, Thermo Fischer Scientific, A11032), goat anti-rabbit IgG (H+L, AlexaFluor 594 conjugated, Thermo Fischer Scientific, A11037) and goat anti-rabbit IgG-HRP (Santa Cruz, sc-2004).

BrdU
<http://www.bdbiosciences.com/ds/pm/tds/555627.pdf>
 GAPDH
<https://www.abcam.com/gapdh-antibody-loading-control-ab22555.html>
 P16
<http://datasheets.scbt.com/sc-56330.pdf>
 Phospho-c-Jun
<https://media.cellsignal.com/pdf/3270.pdf>
 Phospho-GSK3beta
<https://media.cellsignal.com/pdf/5558.pdf>
 Phospho-Akt
<https://media.cellsignal.com/pdf/9271.pdf>
 Phospho-p38MAPK
<https://media.cellsignal.com/pdf/9211.pdf>
 Beta-catenin
<https://www.thermofisher.com/order/catalog/product/RB-9035-P1?SID=srch-srp-RB-9035-P1>
 ACTH
<https://www.fitzgerald-fii.com/acth-antibody-10c-cr1096m1.html>
 Synaptophysin
<https://shop.leicabiosystems.com/us/ihc-ish/ihc-primary-antibodies/pid-synaptophysin>
 MHCII
https://www.novusbio.com/products/mhc-class-ii-i-a-i-e-antibody-m5-114152_nbp1-43312
 CD68
<https://www.abcam.com/cd68-antibody-ab125212.html>
 CD3
https://www.zyto-med.com/storage/uploads/datasheets/en/RBX024_EN.pdf
 B220
<http://www.bdbiosciences.com/eu/applications/research/stem-cell-research/hematopoietic-stem-cell-markers/mouse/negative-markers/purified-rat-anti-mouse-cd45rb220-ra3-6b2/p/553084>
 F4/80
<http://www.bma.ch/en/products/t-2006>
 CD4
<https://www.thermofisher.com/antibody/product/14-9766-80.html?CID=AFLCA-14-9766-80>
 NRas
<https://datasheets.scbt.com/sc-31.pdf>
 Cleaved-caspase 3
<https://media.cellsignal.com/pdf/9664.pdf>
 LINE-1 ORF1p
<https://www.abcam.com/line-1-orf1p-antibody-epr21844-108-ab216324.htm>
 CD8alpha
<https://www.thermofisher.com/order/genome-database/generatePdf?productName=CD8a&assayType=PRANT&detailed=true&productId=14-0808-82>
 CD42b
<https://www.abcam.com/cd42b-antibody-sp219-ab183345.html>
 Ly-6g
<https://www.bdbiosciences.com/us/reagents/research/antibodies-buffers/immunology-reagents/anti-mouse-antibodies/cell-surface-antigens/purified-rat-anti-mouse-ly-6g-1a8/p/551459>
 GLB1
<https://www.ptglab.com/products/GLB1-Antibody-15518-1-AP.htm#validation>
 Ki67
<https://www.abcam.com/ki67-antibody-sp6-ab16667.html>
 GFP
<https://www.chromotek.com/products/detail/product-detail/gfp-antibody-3h9/>

Eukaryotic cell lines

Policy information about [cell lines](#)

Cell line source(s)	IMR90, HEK293T, SK-MEL-5, HCT116, primary bronchial/tracheal epithelial cells, MEFs, MCF7, BNL CL.2 and A549 were purchased from ATCC. HLF and HuH-7 were obtained from JCRB Bank.
Authentication	All human cell lines were authenticated by DNA (STR) profile performed by Eurofins.
Mycoplasma contamination	All cell lines were routinely tested for mycoplasma contamination and were negative.
Commonly misidentified lines (See ICLAC register)	None of the cell lines used in this study is present in the database of commonly misidentified cell lines.

Animals and other organisms

Policy information about [studies involving animals](#); [ARRIVE guidelines](#) recommended for reporting animal research

Laboratory animals	For induction of senescence, both sexes C57BL/6J mice at 8-12 weeks of age were used throughout the study. Female C57BL/6J mice aged 98 to 103 weeks at the start of the experiment and young female C57BL/6J mice (10 weeks old) were used for the ageing experiment. Female C.B-17 SCID/beige were purchased from Charles River and injected at 5-8 weeks of age for HTVI experiment.
Wild animals	No wild animals were used in this study.
Field-collected samples	This study did not involve samples collected in the field.
Ethics oversight	All mouse procedures were performed under licence, following UK Home Office Animals (Scientific Procedures) Act 1986 and local institutional guidelines (UCL or Imperial College ethical review committees).

Note that full information on the approval of the study protocol must also be provided in the manuscript.